JOURNAL OF GEOPHYSICAL RESEARCH, VOL. 112, D23102, doi:10.1029/2007JD008555, 2007

Transport and mixing of chemical air masses in idealized baroclinic life cycles

L. M. Polvani[1] and J. G. Esler[2]

Received 16 February 2007; revised 14 June 2007; accepted 14 August 2007; published 7 December 2007.

[1] The transport, mixing, and three-dimensional evolution of chemically distinct air masses within growing baroclinic waves are studied in idealized, high-resolution, life cycle experiments using suitably initialized passive tracers, contrasting the two well-known life cycle paradigms, distinguished by predominantly anticyclonic (LC1) or cyclonic (LC2) flow at upper levels. Stratosphere-troposphere exchange differs significantly between the two life cycles. Specifically, transport from the stratosphere into the troposphere is significantly larger for LC2 (typically by 50%), due to the presence of large and deep cyclonic vortices that create a wider surf zone than for LC1. In contrast, the transport of tropospheric air into the stratosphere is nearly identical between the two life cycles. The mass of boundary layer air uplifted into the free troposphere is similar for both life cycles, but much more is directly injected into the stratosphere in the case of LC1 (fourfold, approximately). However, the total mixing of boundary layer with stratospheric air is larger for LC2, owing to the presence of the deep cyclonic vortices that entrain and mix both boundary layer air from the surface and stratospheric air from the upper levels. For LC1, boundary layer and stratospheric air are brought together by smaller cyclonic structures that develop on the poleward side of the jet in the lower part of the middleworld, resulting in correspondingly weaker mixing. As both the El Niño-Southern Oscillation and the North Atlantic Oscillation are correlated with the relative frequency of life cycle behaviors, corresponding changes in chemical transport and mixing are to be expected.

Citation: Polvani, L. M., and J. G. Esler (2007), Transport and mixing of chemical air masses in idealized baroclinic life cycles, *J. Geophys. Res.*, *112*, D23102, doi:10.1029/2007JD008555.

1. Introduction

[2] The synoptic-scale circulation associated with developing baroclinic waves acts to transport and mix chemically distinct air masses throughout the extratropical troposphere and the lowermost stratosphere. This transport and mixing strongly influences the climatological distribution of radiatively active trace gases in the upper troposphere and the lower stratosphere, a region which is seen as key to understanding and predicting future climate change [*Holton et al.*, 1995]. The details of transport and mixing are thus fundamental to understanding the response of the atmospheric chemical environment to changes in circulation patterns.

[3] Baroclinic life cycles are well established paradigms for two distinct observed behaviors in the development of nonlinear baroclinic waves [*Thorncroft et al.*, 1993, hereafter THM]. *Shapiro et al.* [1999] have given a detailed description of the relevance of each life cycle type to the observed development of extratropical cyclones. The two basic types of life cycle have been termed 'anticyclonic' (LC1) and 'cyclonic' (LC2) following the dominant sense of the upper level circulation. The anticyclonic life cycle (LC1) is characterized by the development of a strong cold front and slightly weaker warm front, resulting in a 'T-bone' frontal structure. At upper levels the tropopause becomes 'pinched', causing filaments to be sheared out anticyclonically, leading to eventual mixing of stratospheric air into the troposphere. The cyclonic (LC2) life cycle, by contrast, results in the formation of a stronger warm front and a characteristic ''bent-back'' occlusion. At upper levels during LC2-type development, the tropopause rolls-up cyclonically to form a 'cut-off' vortex, as viewed on an isentropic surface, which may subsequently either re-merge with the stratosphere or become mixed into the troposphere. The strong cutoff vortices are associated with the frequently observed 'comma cloud' pattern [*Carlson*, 1980].

[4] The observed transport within an extratropical cyclone/anticyclone pair associated with a developing baroclinic wave typically follows the characteristic pattern sketched in Figure 1, taken from THM. That figure represent airflow on an isentropic surface relative to the motion of the entire system, which is typically moving eastward with characteristic speed of $5-15\ \mathrm{ms}^{-1}$. Details of the relationship between the air mass branches and the synoptic and mesoscale

[1]Department of Applied Physics and Applied Mathematics and Department of Earth and Environmental Sciences, Columbia University, New York, New York, USA.
[2]Department of Mathematics, University College London, London, UK.

0148-0227/07/2007JD008555$09.00

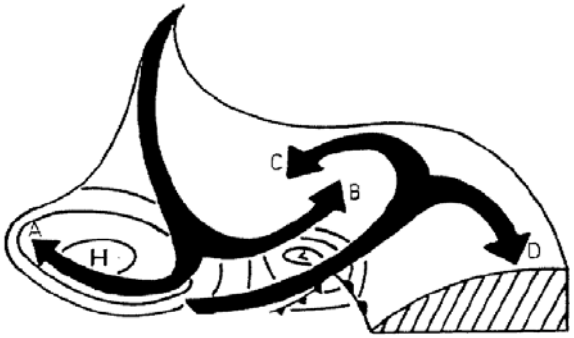

Figure 1. A sketch of relative isentropic flow in a baroclinic life cycle, from *Thorncroft et al.* [1993] (Copyright 1993, Royal Met. Soc. Reproduced with permission).

structure of the developing extratropical cyclone are discussed in the review of *Browning* [1990], and Figure 1 itself is a schematic summary of the work of many authors [see, e.g., *Danielsen*, 1980; *Carlson*, 1980].

[5] Within each developing baroclinic system, two key airstreams are of paramount importance. The first, called the 'warm conveyor belt' lifts boundary layer air upwards and poleward, and is approximately aligned with the surface cold front. The second, referred to as the 'dry intrusion', carries air originating the upper troposphere and lower stratosphere downward and equatorward. As these airstreams encounter stagnation points (in the moving frame of the system) they split into two branches, as can be seen in Figure 1. Branches of the dry intrusion (denoted by the letters A and B) and of the warm conveyor belt (C and D) typically meet and run parallel in three-dimensional 'frontal zones', which are approximately aligned with the developing surface fronts. Large chemical gradients are observable within these frontal zones [e.g., *Bethan et al.*, 1998; *Esler et al.*, 2003; *Mari et al.*, 2004], and the extent and nature of the mixing which takes place between and within adjacent air masses is a subject of ongoing research.

[6] The evolution of air associated with the dry intrusion is also closely related to the development of the tropopause during the passage of the baroclinic wave. As discussed by *Holton et al.* [1995], a mature baroclinic wave may 'break' in a number of ways at the tropopause, leading to exchange of air and constituents between the stratosphere and troposphere. For instance, it is well-established observationally [e.g., *Stohl et al.*, 2003a] that stratospheric ozone and other trace gases are transported into the troposphere when tropopause folds and cut-off cyclones, both features that may develop during baroclinic wave breaking, become irreversibly mixed into the tropospheric environment. Similarly, tropospheric air is frequently observable within the lowermost stratosphere [*Vaughan and Timmis*, 1998; *Hintsa et al.*, 1998; *Ray et al.*, 1999]. In fact, in the lowest part of the lowermost stratosphere the influx of tropospheric air is so frequent that several authors [*Fischer*, 2000; *Hoor et al.*, 2002; *Pan et al.*, 2004] have described this region as a mixing layer, sometimes referred to as the 'extratropical tropopause layer'.

[7] In spite of this wealth of observational evidence and a great many case studies of individual synoptic systems using complex chemical transport models, there has been remarkably little idealized work aimed at carefully quantifying the general features of tracer transport and mixing, specifically in the context of the LC1/LC2 paradigms. The only studies we are aware of are those of *Stone et al.* [1999] who focused on the time evolution of the zonal mean tracer fields in terms of tracer eddy fluxes, *Wang and Shallcross* [2000] who used a Lagrangian trajectory model driven by winds from an idealized GCM experiment, and *von Hardenberg et al.* [2000] who emphasized the chaotic advection surrounding the cut-off vortices in the upper troposphere.

[8] In this paper we aim to greatly extend the above studies by examining in detail the transport and mixing of idealized tracers in canonical baroclinic life cycles of type LC1 and LC2. One crucial difference between this work and earlier studies is that we initialize tracers to correspond, as far as possible, to air masses that have distinct chemical properties in the atmosphere: differences between the evolution and mixing of these idealized tracers may then be argued to be representative of differences in chemical transport and mixing occurring in observed extratropical cyclones. As our numerical experiments involve passive tracers advected by nearly inviscid, adiabatic, dry dynamics, the results presented here must therefore be considered as an idealized starting point.

[9] Broadly speaking, we aim to qualitatively and quantitatively characterize the evolution and mixing of air masses for the canonical LC1 and LC2 life cycles, in the absence of explicit convection, the effects of latent heat release, microphysics, radiation and turbulent mixing processes. Specifically, we aim to address the following questions:

[10] • How does stratosphere-troposphere exchange differ between LC1 and LC2? In particular, does each life cycle have a different characteristic ratio of stratosphere to troposphere transport relative to troposphere to stratosphere transport? What is the vertical structure of these transports? For instance, does one life cycle inject tropospheric air into the lowermost stratosphere at significantly higher levels compared to the other? This question is clearly important for the chemical impact of tropospheric trace gases on lower stratospheric ozone, for example, since there is a strong vertical gradient in ozone mixing ratio within the lowermost stratosphere. The depth of the 'extratropical tropopause layer' discussed above may therefore also be sensitive to the type of life cycle preferred in a particular season.

[11] • Does the uplifting of boundary layer air to the free troposphere differ significantly between the two types of life cycle? Is significant boundary layer air injected directly into the lowermost stratosphere in either life cycle, as trajectory studies suggest may occur in observed extratropical cyclones [*Stohl et al.*, 2003b]? At which levels is this boundary air injected? The chemical impact of a range of species emitted in the extratropics, including very short-lived halogenated species [*Law et al.*, 2007] may depend critically on the answers to the above, as transport within an extratropical cyclone may provide a mechanism to rapidly bring such species into contact with ozone-rich air in the lowermost stratosphere.

[12] • Can the three-dimensional transport of tracers within idealized life cycles be reconciled with the schematic model of relative isentropic motion shown in Figure 1? In

Table 1. Values of the Parameters Used in This Study

Parameter	Value	Units
g	9.806	m/s^2
a	6.371×10^6	m
Ω	7.292×10^{-5}	1/s
R	287	J/kg/K
κ	2/7	
c_p	R/κ	J/kg/K
p_0	10^5	Pa
H	7.5	km
U_0	45	m/s
z_T	13	km
U_s	45	m/s
ϕ_s	35	degrees
Δ_s	20	degrees
z_s	10	km
T_0	300	K
Γ_0	−6.5	K/km
α	10	
$\hat{T}$	1	K
$\hat{\phi}$	$\pi/4$	radians
m	6	

other words, what does Figure 1 look like when it is *computed* rather than *sketched*? How does it differ between LC1 and LC2? Does the computed three-dimensional picture add new elements which are not present in the common isentropic view?

[13] To answer these questions, a set of idealized experiments, using a numerical model to solve the dry primitive equations on a sphere, are described in Section 2 below. In Section 3 the initial distribution of the idealized tracers, chosen to be representative of chemically distinct air masses, is presented together with appropriate diagnostics of transport and mixing. In Section 4 the time-evolution of the tracers and diagnostics relevant to stratosphere-troposphere exchange are described, and in Section 5 results relating to transport from the boundary layer to the free troposphere and stratosphere are presented. In Section 6 the three-dimensional evolution of the tracer fields are investigated, with reference to the schematic models of relative isentropic motion discussed above. A summary and some conclusions are offered in the final section.

2. Life Cycle Dynamics

[14] In order to study the detailed characteristics of tracer transport and mixing during baroclinic life cycles, two distinct ingredients are necessary. First, we need to set up the dynamics that faithfully reproduce the well known behavior of the canonical life cycle types. Second we need to initialize tracers so that they are representative of distinct air masses (e.g., boundary layer air or lower stratospheric air); the placement of initial tracers is crucial the evaluation of transport, e.g., across the tropopause. We discuss the dynamics in this section, and the initial placement of tracers in the following one.

2.1. Equations

[15] Our dynamical model consists of the nearly inviscid, dry, adiabatic primitive equations on the sphere. In σ coordinates [*Durran*, 1999] the horizontal velocity $\mathbf{u} = (u, v)$, the temperature T and the surface pressure p_s obey

$$\begin{aligned} &\frac{d\mathbf{u}}{dt} + f\mathbf{k}\times\mathbf{u} + \nabla_h\Phi + \frac{RT}{p_s}\nabla_h p_s = \nu\nabla_h^6\mathbf{u} \\ &\frac{dT}{dt} - \frac{\kappa T}{\sigma p_s}\omega = \nu\nabla_h^6 T \\ &\frac{\partial p_s}{\partial t} + \int_{\sigma_T}^{1} \nabla_h\cdot(p_s\mathbf{u})d\sigma = 0 \end{aligned} \tag{1}$$

where all the notation is standard. Recall that $f = 2\Omega\sin\phi$ is the Coriolis parameter (ϕ being the latitude), ∇_h denotes the horizontal gradient operator, and $\sigma \equiv p/p_s$, where p is the fluid pressure. Values of the physical constants used in this study are given in Table 1. The geopotential Φ and the pressure vertical velocity ω are computed using the diagnostic relationships

$$\Phi = R\int_{\sigma}^{1}\frac{T}{\sigma'}\,d\sigma' \tag{2}$$

and

$$\omega = \sigma\mathbf{u}\cdot\nabla p_s - \int_{\sigma_T}^{\sigma}\nabla\cdot(p_s\mathbf{u})d\sigma' \tag{3}$$

and the material derivative is defined by

$$\frac{d}{dt} = \frac{\partial}{\partial t} + \mathbf{u}\cdot\nabla + \dot{\sigma}\frac{\partial}{\partial\sigma}. \tag{4}$$

The model surface (σ = 1) is flat, and the model top is located at $\sigma = \sigma_T$. The boundary conditions at the model top and surface are simply $\dot{\sigma} = 0$.

2.2. Numerics

[16] Solutions to the primitive Equation (1) are computed using GFDL's Flexible Modeling System (FMS) Spectral Dynamical Core (using the "Jakarta" release version). This uses a pseudo-spectral transform method in the horizontal, a Simmons-Burridge finite difference method in the vertical, and a Robert-Asselin filtered semi-implicit Crank-Nicholson/leapfrog scheme for time integration; all these techniques are standard. The hyperdiffusion terms on the right hand side of (1) are needed to control the enstrophy cascade, and the value of ν (which depends on the horizontal resolution) is chosen so as to capture progressively finer scales as the resolution is increased.

[17] The extent of the vertical domain we choose for our calculations is dictated by the fact that, among other things, we are interested in quantifying stratosphere-troposphere exchange. We thus place the top of the computational domain at $\sigma_T = 0.02$, which corresponds to roughly 30 km; the tropopause is then located in the middle of the domain (and not near the top, as is often the case). This choice also means that the model top is sufficiently far from the region of interest, that the boundary condition $\dot{\sigma} = 0$ at $\sigma = \sigma_T$ does not affect the results (note: there are no sponge layers near the model top). Furthermore, in order to properly resolve the tropopause region, the model levels are not equally spaced in σ (as is customary), since that would yield sparse levels

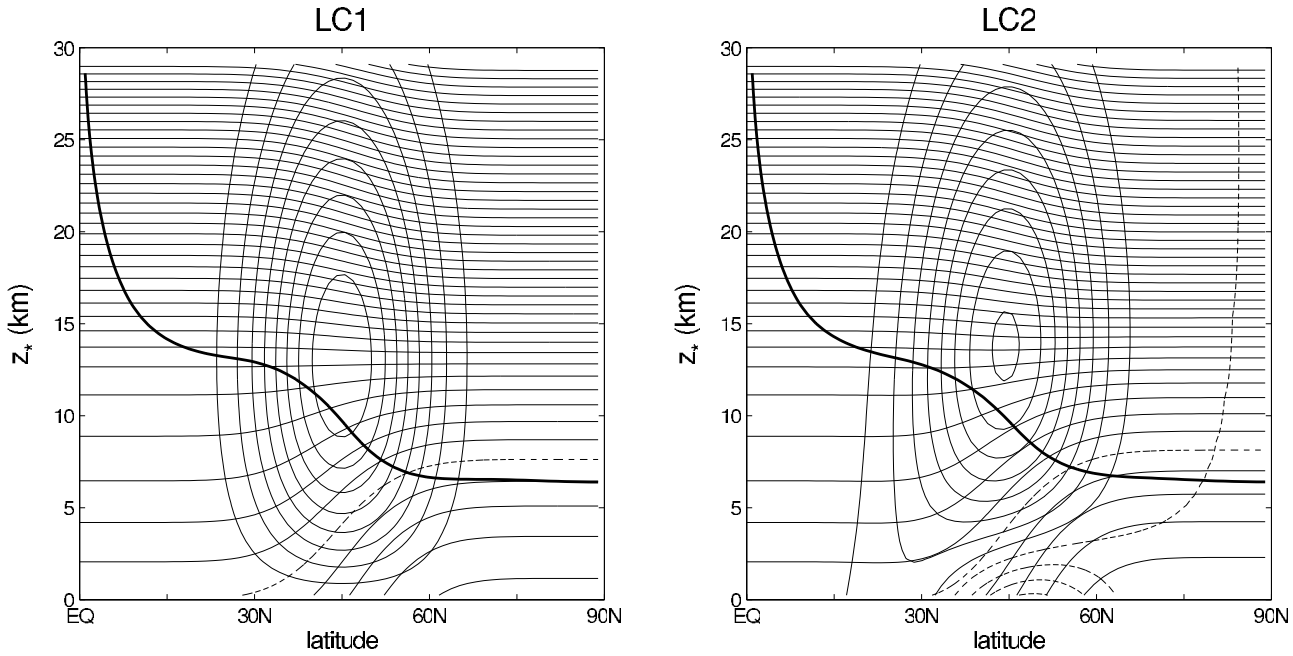

Figure 2. Initial conditions for life cycles LC1 (left) and LC2 (right). Winds: 5 ms^{-1} contour interval, with zero and negative contours dashed. Potential temperature: 10 K contour interval, with the 300 K isentrope dashed. The bold line indicates the position of the 2 PVU surface.

around the tropopause and above. We chose, instead, to compute with equal resolution at all heights, and thus set the model levels to be equally spaced in $\log(\sigma)$.

[18] It is very important to establish the degree to which the computed results regarding transport and mixing are dependent on the vertical (Δz) and horizontal (Δx) grid size. To do this, one needs to refine the horizontal and vertical grids in a consistent way. As we are computing large scale, balanced motions, the obvious choice is to require that $\Delta x/\Delta z = f/N$, where N is the Brunt-Vaissala frequency. Evaluating this expression for the Coriolis parameter at 45°, around which our life cycles are centered, yields the simple formula [*Lindzen and Fox-Rabinowitz*, 1989]

$$\Delta z = \frac{\Omega a}{N}\Delta\phi \tag{5}$$

where a is the Earth's radius. Keeping in mind that the stratosphere occupies half of our computational domain, we choose $N = 0.02\ s^{-1}$, and use the values of Ω and a as given in Table 1. For triangular truncation with maximum wave number 42, with 128 equally spaced grid points along each latitude circle, corresponding to $\Delta\phi \approx 2.8°$, the above formula gives $\Delta z \approx 1$ km. As we have placed the model top near 30 km (approximately 20 hPa), we need 30 vertical levels at this horizontal resolution. We use the short hand "T42L30" to refer to this coarsest resolution. We have doubled and quadrupled this resolution, and thus computed all solutions at T42L30, T85L60 and T170L120. Unless otherwise stated, all the figures below show the solution at T170L120 resolution, for which the vertical level spacing is 250 m, and the horizontal grid spacing is 0.7°.

2.3. Initialization

[19] Our goal is to set up and initial flow so as to faithfully replicate the two paradigms of life cycle behaviors, as discussed in THM. Unfortunately, THM do not analytically specify their initial conditions, and we are thus unable to reproduce their work identically. Nonetheless, it is relatively easy to construct analytical expressions that yield the desired behavior.

[20] For an LC1 life cycle, we pick a zonal wind profile u_1 that mimics very closely the THM initial condition, using the simple function

$$u_1(\phi, z) = U_0\ F(\phi)\left[(z/z_T)e^{-\left[(z/z_T)^2-1\right]/2}\right] \tag{6}$$

where the log-pressure height $z \equiv H\log p_0/p$ is simply a proxy for the pressure p. The latitudinal dependence is chosen to be, following *Simmons and Hoskins* [1977]

$$F(\phi) = \begin{cases} \left[\sin\left(\pi(\sin\phi)^2\right)\right]^3 & \text{for } \phi > 0 \\ 0 & \text{for } \phi < 0. \end{cases} \tag{7}$$

Note that, while not strictly analytic, this function is very smooth at the equator. Expression (6) is a two parameter function, with a maximum wind velocity U_0 at z_T, and simple latitudinal envelope that peaks at $\phi = 45°$N. For the values of U_0 and z_T given in Table 1, these expressions yield an excellent match to the LC1 initial condition in THM. This can be seen in Figure 2 (left panel), where the jet at 200 hPa (approximately 12 km) has a speed of 45 ms^{-1}.

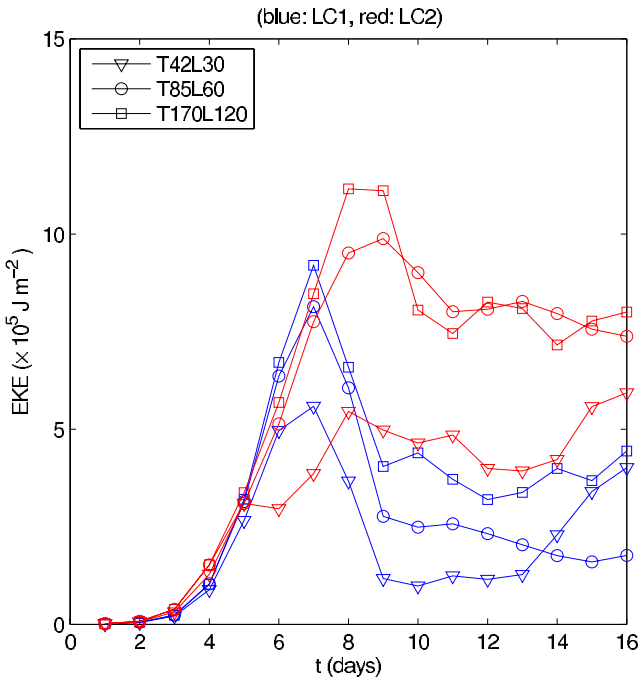

Figure 3. Eddy kinetic energy versus time. Blue curves for LC1, red for LC2. Different symbols denote different resolutions (see legend).

[21] For a life cycle of type LC2 the zonal wind profile u_2 is chosen, following THM, by modifying u_1 so as to add a meridional shear u_s to expression (6) above, i.e.

$$u_2(\phi, z) = u_1(\phi, z) + u_s(\phi, z). \tag{8}$$

Following *Hartmann* [2000] we confine u_s to the lower troposphere, the region that most directly influences the type of life cycle that appears, and set

$$u_s(\phi, z) = -U_s \; e^{-z/z_s} [\sin(2\phi)]^2 \left[\frac{\phi - \phi_s}{\Delta_s}\right] e^{-\left[\frac{\phi-\phi_s}{\Delta_s}\right]^2} \tag{9}$$

where the values of the parameters U_s, ϕ_s, Δ_s and z_s are given in Table 1. The resulting winds are shown in the right panel of Figure 2. As we will demonstrate below, these choices lead to an LC2 that is clearly distinct from the LC1 in terms of the cyclonic features near the tropopause. For both LC1 and LC2, the initial meridional velocity $v = 0$.

[22] For both life cycles, given the above winds, we then compute a temperature T and a surface pressure p_s that are in exact balance with the corresponding winds field. This is easily accomplished, but is not entirely trivial; notably, a nonlinear iterative procedure is needed to compute the initial p_s for case LC2. While these balancing procedures are surely not new, we were unable to find them detailed in the literature. Therefore for the sake of completeness and reproducibility, we have included them in the Appendix. As shown there, one may add any ϕ-independent component to the balanced temperature field. To reflect the gross structure of the observations, a profile with a distinct jump in the Brunt-Vaissala frequency around the tropopause is chosen. The resulting initial potential temperature $\theta = T\,(p_0/p)^{\kappa}$, for both LC1 and LC2, is shown in Figure 2; notice that the density of θ contours above the tropopause is noticeably higher than in the troposphere.

[23] The purely zonal initial flow just described, while baroclinically unstable, is in perfect balance. In order to generate a life cycle, some perturbation is required. THM computed the most unstable linear normal mode of the balanced flow, and used that as the initial perturbation. This procedure is not only computationally cumbersome (as a non-constant-coefficient eigenvalue problem needs to be solved numerically), but also unnecessary. Here, for the sake of simplicity and reproducibility, the instability is induced by perturbing the temperature field alone by a small amount T', which is independent of height and has the following functional form:

$$T'(\lambda, \phi) = \hat{T} \cos(m\lambda) \quad \left[\operatorname{sech}\left(m\left(\phi - \hat{\phi}\right)\right)\right]^2; \tag{10}$$

where λ is the longitude. As with THM, we set $m = 6$ and exploit the ability of our pseudo-spectral code to compute only multiples of that longitudinal wave number. As in the work of *Polvani et al.* [2004], we did not find it necessary to balance this tiny perturbation ($T' = \hat{T} = 1$ K at $\hat{\phi} = 45°$N, the jet maximum). The small initial imbalance is very rapidly overwhelmed by the most unstable normal mode, which completely controls the evolution of the flow. As in THM, we integrate the model equations for 16 days, by which time the lifecyles are complete, as illustrated by the eddy kinetic energy which we discuss next.

2.4. Evolution

[24] The primitive equations (1), when initialized as described, generate life cycles that are indistinguishable, in most respects, to the paradigms in THM. This is seen first in Figure 3, where the eddy kinetic energy (EKE) of the two life cycles is plotted versus time. This figure may be directly compared with Figure 4 in THM. While the specific values of EKE depend on resolution, the qualitative character of the curves does not. Note, in particular, how LC2 peaks somewhat later and at larger amplitude than LC1, and how the level of EKE for LC2 remains high even after the life cycle has completed. This is due to the well known fact that strong cyclonic centers persist in the LC2 case.

[25] The top row of Figure 4 shows Ertel potential vorticity (PV) on the 335 K isentropic surface, which is located at the center of the "middleworld" (see below), and the bottom row shows the temperature field at the surface (the lowest model level). The left column shows the fields for LC1 at day 7, and the right column for LC2 at day 8; these were chosen to best illustrate the features of the two life cycle types, and roughly correspond to the days when EKE reaches a maximum in each case. In this and all subsequent figures plotted in a latitude-longitude domain, we use a conic Albers equal-area projection [*Snyder and Voxland*, 1994], with standard parallels at 30°N and 60°N. The reason for choosing an equal-area type projection will become apparent below: it will enable us to graphically compare the relative areas of different tracer regions.

[26] The PV field in the top row of Figure 4 shows the familiar characteristics of each life cycle, with anticyclonic tongues of stratospheric air breaking equatorward for LC1

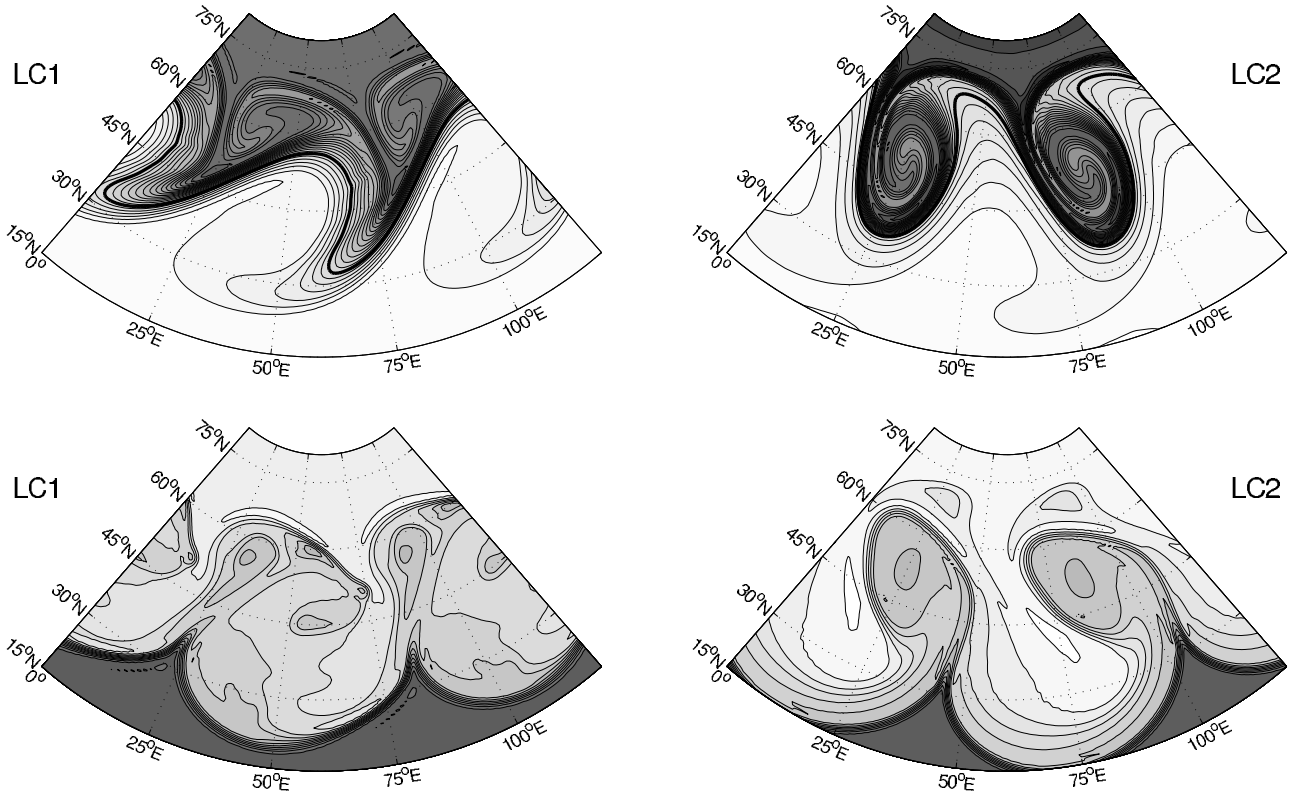

Figure 4. Ertel PV on 335 K (top row) and surface temperature (bottom row) at day 7 for LC1 (left) and day 8 for LC2 (right). For PV: contour interval of 0.25 PVUs, with the 2 PVU contour in bold. Temperature: contour interval of 4 K. The projection is Albers Equal Area, with standard parallels at 30°N and 60°N.

and cyclonic cutoff vortices for LC2. These can be contrasted with the corresponding figure of potential temperature on the 2 PVU surface in THM. Note, in addition, that in each life cycle type one can detect, albeit in smaller measure, the characteristics of the other type. For instance, in LC1 one can clearly see cyclonic vortices being formed poleward of the typical anticyclonic tongues; similarly, the outermost PV contours in LC2 can be seen turning in an anticyclonic sense. The key point here is that, while LC1 and LC2 are paradigmatic examples, observed extra-tropical cyclones will exhibit feature of both types of life cycle: there is no such thing as a "pure" LC1 or a "pure" LC2.

[27] The surface temperature fields for LC1 and LC2, shown in the bottom row of Figure 4, illustrate the development of the surface fronts in each life cycle. The key features are very similar to those in THM's Figure 5 (day 7) and Figure 8 (days 8–9), even though our life cycles were computed from simple, analytical, and thus completely reproducible initial conditions. Hence we are ready to discuss the initialization of the tracers.

3. Tracer Initialization and Diagnostics

3.1. Initialization

[28] Unlike the previous studies mentioned in the introduction, one goal of this work is to quantify the amount of mixing that occurs between air masses of different origin in idealized baroclinic life cycle. In order to accomplish this, we advect a number of different tracers, initially located so as to be representative, as far as possible, of air masses with distinct physical and chemical properties. The initial placement of the tracers used in this study is shown in Figure 5. We emphasize that this figure is not a sketch.

[29] We start, in the spirit of *Hoskins* [1991], by defining the "middleworld" as the region the atmosphere located the 290 K and 380 K isentropic surfaces. We further divide it into three sub-regions, spaced 30 K apart (indicated by the solid red lines in Figure 5) in order to be able to quantify, albeit crudely, the vertical structure of the transport and mixing in each life cycle.

[30] Next we need to define a tropopause, so as to differentiate tropospheric from stratospheric air. A naive way to proceed would be to pick the tropopause to correspond, for instance, to the 2 PVU surface (one PVU equals 10^{-6} m^2 s^{-1} K Kg^{-1}). While this value approximately corresponds to the dynamical tropopause in observational analyses [see, e.g., *Berthet et al.*, 2007], it would be meaningless to use this definition here, given our idealized winds. A more dynamically minded definition, which we are able to adopt here given the nearly adiabatic nature of our dynamics, is to define the tropopause as the latitude, on each isentropic surface, where *PV gradients* are the largest. As *McIntyre and Palmer* [1984] have suggested, one may view the tropopause as the edge of the region of potential vorticity mixing (the "surf zone") on each isentropic surface.

[31] Thus we compute on each isentropic surface from 290 K to 380 K, in steps of 10 K, the location of the

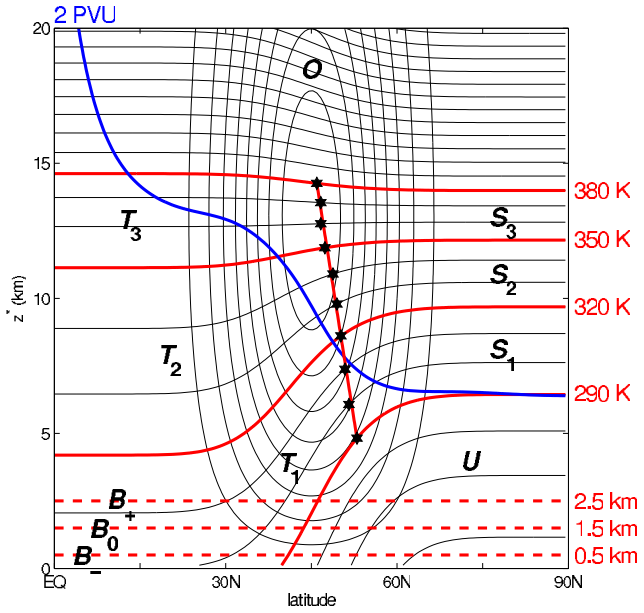

Figure 5. Initial location of the tracers used in this study. Thin black lines: u and θ, as in Figure 2. Solid red lines: boundaries of the tracer domains, as detailed in Table 2. The asterisks show the location of maximum PV gradient on each isentropic surface. Each tracer is initialized with a value of 1 in its specified domain, and 0 elsewhere. Dashed red line: boundary layer tracers, initialized to 1 below the line and 0 above. Blue line: the 2 PVU surface.

maximum potential vorticity gradients. These are indicated by the asterisks in Figure 5. In order to make the placement of tracers easier for us and, more importantly, reproducible by other investigators, we then simply interpolate the asterisks with a straight line. This yield a simple analytic expression for the height Z_T (in km) of the dynamically based tropopause as a function of the latitude φ_T (in degrees) in the middleworld

$$Z_T(\varphi_T) = \left(\frac{3}{2}\right)(55 - \varphi_T) \quad \text{for} \quad 290 \le \theta \le 380 \qquad (11)$$

Alternatively, one may think of this expression as a definition of latitude φ_T of the tropopause at each height, and thus on each isentropic surface. Note that such a tropopause, defined from the maximum PV gradients along isentropic surfaces, is a lot steeper that the 2 PVU surface (the blue curve in Figure 5).

[32] Armed with the simple expression (11) for the tropopause in the middleworld, we now lay down 8 different tracers, meant to cover all key regions of the atmosphere. All tracers are given initial values of 1 in their initial domains, and 0 elsewhere.

[33] As illustrated in Figure 5, tracers O and U mark "overworld" and "underworld" air (in the sense of *Hoskins* [1991]), and are nonzero above 380 K and below 290 K, respectively. In the middleworld we place 6 tracers, three on each side of the tropopause. Tracers T_i (i = 1, 2, 3) are used to mark tropospheric air, and tracers S_i are used for stratospheric air, as detailed in Table 2.

[34] Since, in addition to stratosphere-troposphere exchange, we are interested in the fate of air injected from the boundary layer into the free troposphere and eventually the stratosphere, we also advect three boundary layer tracer (dashed red curves in Figure 5). The one labeled B_0 is initially located between the model surface and z = 1.5 km; it is meant to represent a canonical boundary layer with a depth of 1.5 km. The quantitative dependence of the results on the depth the boundary layer, is explored via the tracers B_+ and B_-, which are initially located between the model surface and 2.5 and 0.5 km, respectively.

[35] Finally, a word about the tracer advection scheme. Our dynamics is computed using a standard pseudo-spectral scheme, but this is obviously inadequate for tracer advection. Hence we use a piecewise linear van Leer scheme for both horizontal and vertical advection. Owing to the fact that log surface pressure is the prognostic variable, tracer mass is not exactly conserved by our numerical scheme. However, as *Galewsky et al.* [2005] have shown, the accumulated error for such a scheme is exceedingly small for the total mass, of the order of 1% over a timescale of a year at T42 resolution; our calculations are much shorter than that. Furthermore, we have validated our results by computing the solution at double and quadruple resolution, both horizontally and vertically, and are therefore confident that our computations are robust.

3.2. Diagnostics

[36] One of the advantages of having defined our tracers to initially correspond to distinct air masses is that the tracers *themselves* can be then used to define distinct regions of the atmosphere at subsequent times. This greatly facilitates calculation of transport, notably cross-tropopause transport. Traditional methods of computing such transport are well known to be unreliable, being very sensitive to both interpolation errors and numerical resolution [*Wirth and Egger*, 1999; *Gettelman and Sobel*, 2000; *Wernli and Bourqui*, 2002]. In addition, they may require the cumbersome computation, for instance, of the tropopause surface in terms of PV values, and of fluxes across that surface [*Wei*, 1997].

[37] In this study transport is very easily calculated, since different regions of the atmosphere can be immediately identified from the values of the tracers themselves. To accomplish this, we start by defining a stratospheric tracer S

$$S = S_1 + S_2 + S_3 + O, \qquad (12)$$

Table 2. The Tracers Used in This Study, and Their Initial Domains[a]

Tracer	Initial Domain	Airmass
O	$\theta > 380$	overworld
U	$\theta < 290$ and $\varphi > 0$	underworld
T_1	$350 < \theta < 380$ and $\varphi > \varphi_T$	high middleworld trop.
T_2	$320 < \theta < 350$ and $\varphi > \varphi_T$	center middleworld trop.
T_3	$290 < \theta < 320$ and $\varphi > \varphi_T$	low middleworld trop.
S_1	$350 < \theta < 380$ and $\varphi < \varphi_T$	high middleworld strat.
S_2	$320 < \theta < 350$ and $\varphi < \varphi_T$	center middleworld strat.
S_3	$290 < \theta < 320$ and $\varphi < \varphi_T$	low middleworld strat.
B_+	$0 < z < 2.5$ km	high boundary layer
B_0	$0 < z < 1.5$ km	canonical boundary layer
B_-	$0 < z < 0.5$ km	low boundary layer

[a]The latitude φ_T is defined implicitly via equation (11). At t = 0, the tracers are given a value of 1 inside their respective domains, and 0 elsewhere.

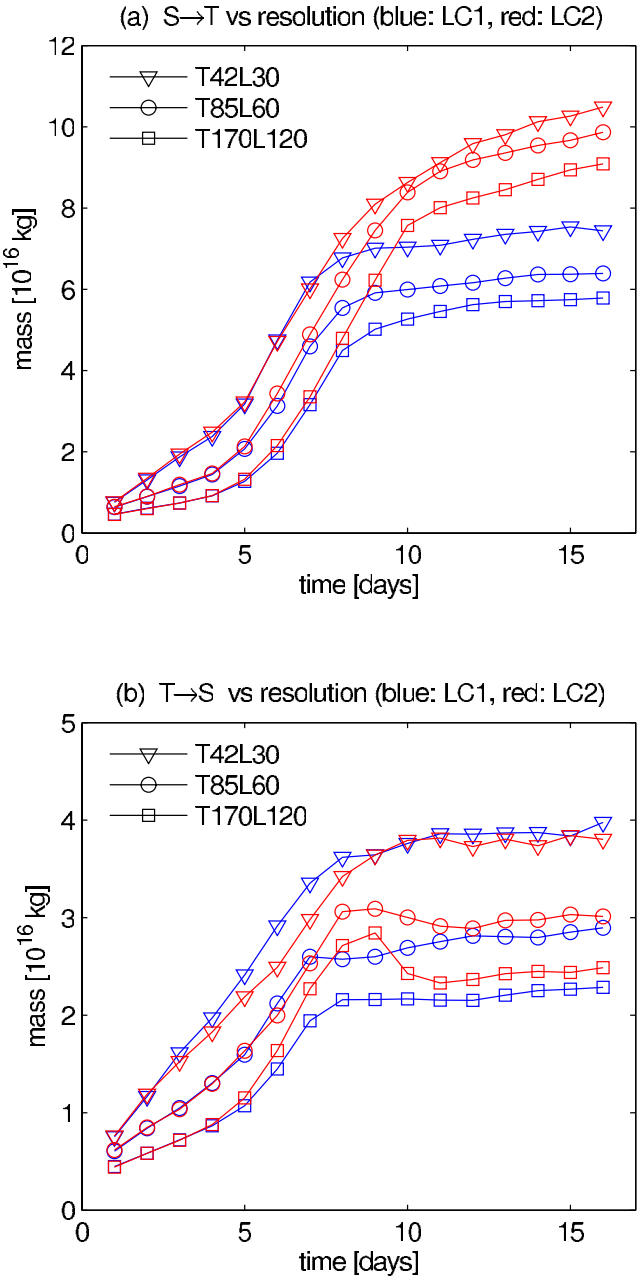

Figure 6. Vertically integrated mass transport across the tropopause as a function of time. (a) $S \rightarrow \mathcal{T}$ and (b) $T \rightarrow \mathcal{S}$, as defined in Equations (14) and (15), respectively. Blue lines indicate life cycles of type LC1, red lines of type LC2. Different symbols correspond to different resolutions, as indicated in the accompanying legends.

and a tropospheric tracer T

$$T = T_1 + T_2 + T_3 + U. \tag{13}$$

It should be clear that $T = 1 - S$, by construction, everywhere and at all times. From this it follows that the stratosphere $\mathcal{S}$ can be defined simply as the region where $S > 0.5$, and similarly the troposphere $\mathcal{T}$ as the region where $T > 0.5$. The isosurface $T = S = 0.5$ then becomes the natural definition of the tropopause. Although the actual shape of this surface becomes rather complicated as the life cycle evolves, it can be computed very simply.

[38] A very natural definition of cross-tropopause transport follows from the above. We define $S \rightarrow \mathcal{T}$, the transport from the stratosphere to the troposphere, as

$$S \rightarrow \mathcal{T} = \int_{\mathcal{T}} S \, \rho dV \tag{14}$$

where $\mathcal{T}$ designates the troposphere as defined above. Similarly $T \rightarrow \mathcal{S}$, the troposphere to stratosphere transport, is defined by

$$T \rightarrow \mathcal{S} = \int_{\mathcal{S}} T \, \rho dV. \tag{15}$$

These definitions have the advantage that they are extremely easy to compute in practice (e.g., using masks), and no differentiation and/or interpolation is needed to compute the transport across any time-dependent and complex interface (e.g., the tropopause). The only caveat is that, in order to minimize spurious transport of numerical origin in the equatorial regions and the other hemisphere, the volume integrals in these expressions (and similar ones below) are confined to latitudes from 15°N to the pole.

[39] Variations on these definitions, based on the tracers defined above, can be used to examine the vertical structure of the stratosphere-troposphere exchange, transport out of the boundary layer, and mixing between boundary layer and stratospheric air. The specific expressions are introduced as needed in the relevant sections below.

4. Stratosphere-Troposphere Exchange

[40] Having described the dynamical evolution of our life cycles and the initialization of the tracers corresponding to the various air masses, we now turn to a detailed characterization of stratosphere-troposphere exchange within idealized baroclinic life cycles. We here consider both the transport from the stratosphere into the troposphere ($S \rightarrow \mathcal{T}$) and the reverse ($T \rightarrow \mathcal{S}$), and examine the vertical structure of these quantities by looking at various isentropic layers in the middleworld. From these we determine the key qualitative and quantitative differences between life cycles of type LC1 and those of type LC2.

[41] The time evolution of $S \rightarrow \mathcal{T}$ over the life cycle is shown in Figure 6a. In this and similar figures below, blue lines correspond to life cycles of type LC1, and red lines to type LC2. Different symbols designate different numerical resolutions. The first result of this study is immediately apparent from that figure: LC2 life cycles are considerably more efficient then LC1 life cycles at transporting air from the stratosphere into the troposphere. Note that while the actual values of the mass transport are quite sensitive to model resolution, the key result is robust: $S \rightarrow \mathcal{T}$ for LC2 life cycles is approximately 1.5 times greater than for LC1, irrespective of resolution. In contrast, the transport $T \rightarrow \mathcal{S}$ into the stratosphere differs little between the two types of life cycle, as can be seen in Figure 6b. Again, this is a robust result, since is independent of model resolution. In order to understand these results, one needs to look in detail at the tracers in the middleworld.

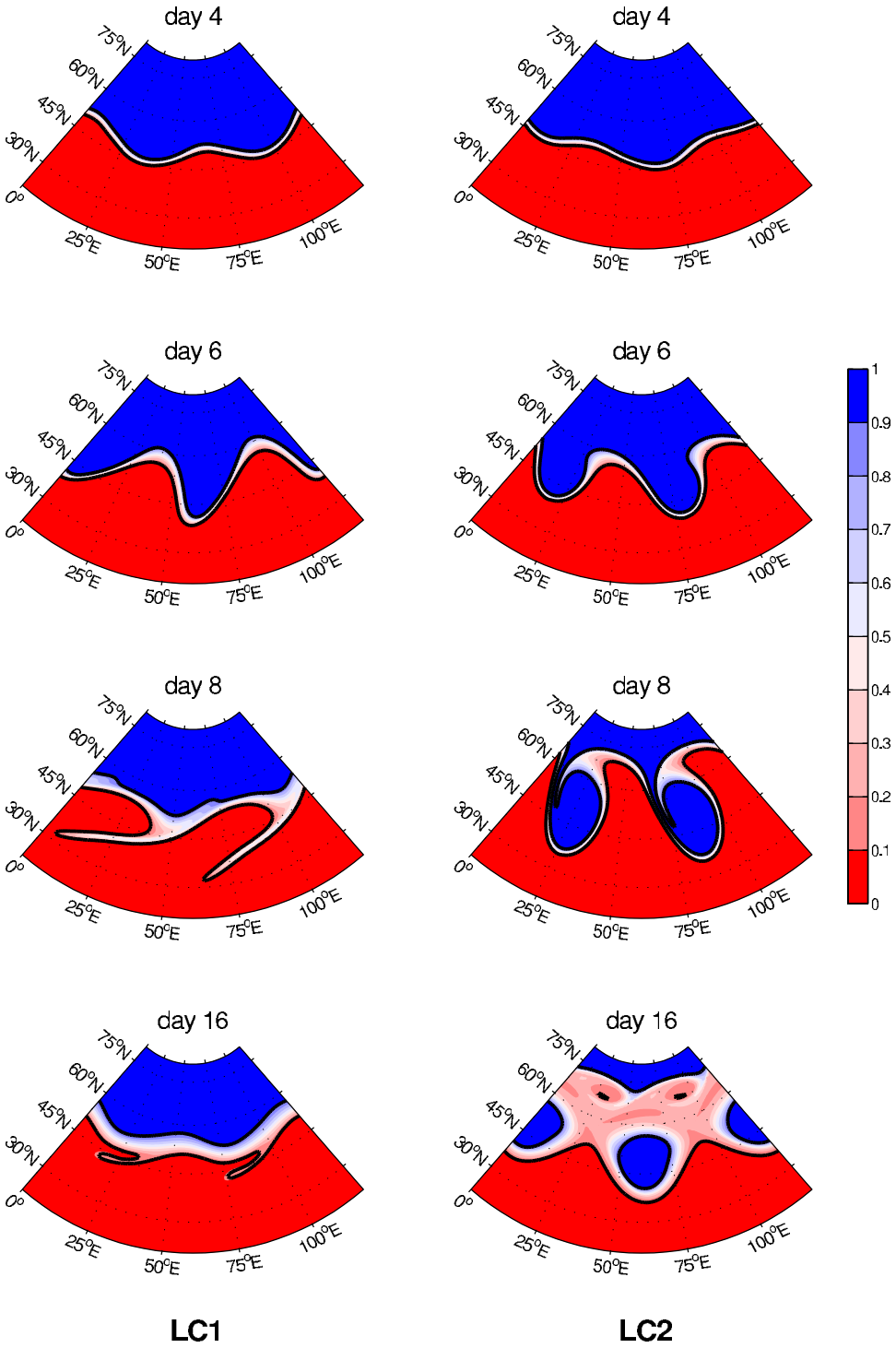

Figure 7. Tracer evolution, at selected days, on the isentropic surface θ = 335 K from the T170L120 solution; left column for the LC1 life cycle, right column for LC2. Color shading indicates the value of tracer S, as defined in Equation (12); hence, blue denotes stratospheric air, and red tropospheric air. The thick black lines mark the locations where the product of tracers S and T is equal to 0.1, delimiting the mixing zone described in the text. As in Figure 4, the projection is Albers Equal Area, with standard parallels at 30°N and 60°N.

[42] In Figure 7, the evolution of the tracers on the 335 K isentropic surface is shown, with the LC1 life cycle on the left, and the LC2 life cycle on the right. The color-shaded quantity is the stratospheric tracer S, defined in Equation (12). The palette is chosen so that blue corresponds to values of $S > 0.5$, and red to $S < 0.5$ (which is equivalent to $T > 0.5$): in simple terms, blue shows stratospheric air and red tropospheric air. The thick black contours show the location

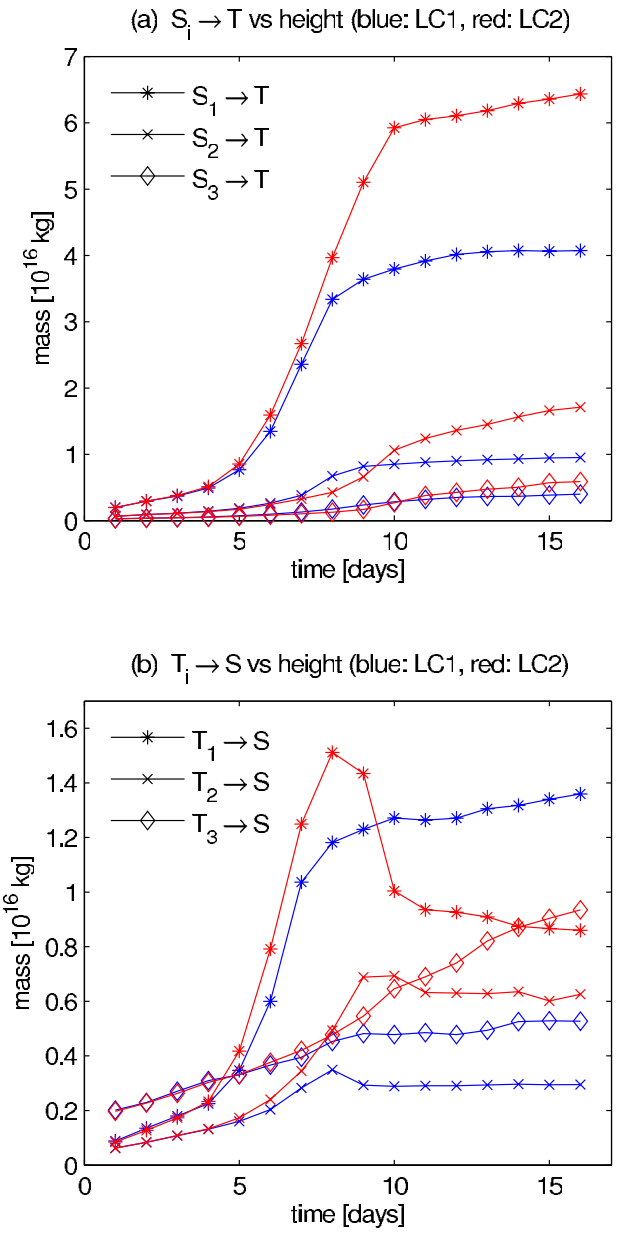

Figure 8. Layerwise mass transport across the tropopause as a function of time, for the T170L120 solutions. (a) $S_i \rightarrow \mathcal{T}$ and (b) $T_i \rightarrow \mathcal{S}$, as defined in Equations (16) and (17), respectively. Blue lines indicate life cycles of type LC1, red lines of type LC2. Different symbols correspond to different layers in the middleworld (cf. Figure 5), as indicated in the accompanying legends.

where the product $S \times T = 0.1$. In the latitudinal band enclosed between these two contours the value of the product is larger than 0.1; this is where most of the mixing occurs between the stratospheric and tropospheric air masses: we refer to it as the "mixing zone". It is worth mentioning that very little cross-isentropic transport occurs in our high-resolution computations. In fact, if tracer S_2 is plotted instead of the tracer S, all the features in Figure 7 are unchanged (indistinguishably to the eye); this confirms that there is very little numerical leakage of tracers S_1 and S_3 onto the 335 K surface (cf. Figure 5). With this in mind, three key feature of tracer transport and mixing in life cycles should be noted.

[43] First, the tracers in Figure 7 evolve as might be expected from the canonical properties of the two life cycles (cf. the top row of Figure 4, where Ertel PV is shown on the same 335 K surface). For life cycle LC1, a thin filament of stratospheric air is pinched off the breaking baroclinic wave and is subsequently advected anticyclonically and mixed into the troposphere. In LC2, by contrast, the breaking wave rolls up cyclonically to form cut-off vortices that contain unmixed stratospheric air; because they are relatively large and coherent, these vortices are able to stir a large portion of the lowermost stratosphere into a large mixing zone, as can be seen from the bottom-right panel in Figure 7. Hence stratosphere-troposphere exchange occurs in both life cycles, but in very different and characteristic fashions.

[44] Second, the direction of stratosphere-troposphere exchange can be directly inferred from Figure 7. The color in the mixing regions is primarily red (this is particularly clear for the LC2 case at late times). This means that the mixed air is located mostly in the troposphere, and one therefore expects $S \rightarrow \mathcal{T}$ to be larger than $T \rightarrow \mathcal{S}$, as validated in Figure 6. We note *en passant* that the ratio of $(T \rightarrow \mathcal{S})/(S \rightarrow \mathcal{T})$, at the end of each life cycle, is approximately 0.4 for LC1 and 0.27 for LC2 (at T170L120). While our life cycles are highly idealized, notably by the complete absence of moist and convective processes, these numbers are similar with those estimated from observations, e.g., *Wirth and Egger* [1999], using standard methods.

[45] Third, one can immediately see from Figure 7 that $S \rightarrow \mathcal{T}$ is considerably greater for LC2 life cycles than for LC1. The mixing region produced by the strong cyclonic vortices in the LC2 case extends, roughly, from 40°N to 75°N, whereas for LC1 the mixing region is less than 10° wide. Since we have plotted the tracers using an equal-area projection, one might expect $S \rightarrow \mathcal{T}$ to be roughly a factor of 3 greater for LC2 than for LC1. This value, however, is about twice as large as the value 1.5 reported in Figure 6. The discrepancy is easily resolved if one keeps in mind that Figure 7 only shows a single isentropic surface in the middleworld, and may therefore not be entirely representative of the tracer evolution at other levels. Thus the vertical structure of the mixing needs to be examined in more detail.

[46] This is explored in Figure 8, where the layerwise cross tropopause transport for both LC1 and LC2 life cycles is plotted. Specifically, we have computed the quantities

$$S_i \rightarrow \mathcal{T} = \int_{\mathcal{T}} S_i \, \rho dV \tag{16}$$

and

$$T_i \rightarrow \mathcal{S} = \int_{\mathcal{S}} T_i \, \rho dV \tag{17}$$

for $i = 1, 2, 3$. These quantities are representative of the cross-tropopause transport in the lower, middle and upper layers of the middleworld, respectively (cf. Figure 5). One can therefore determine the importance of different regions of the lowermost stratosphere to the net transport into the

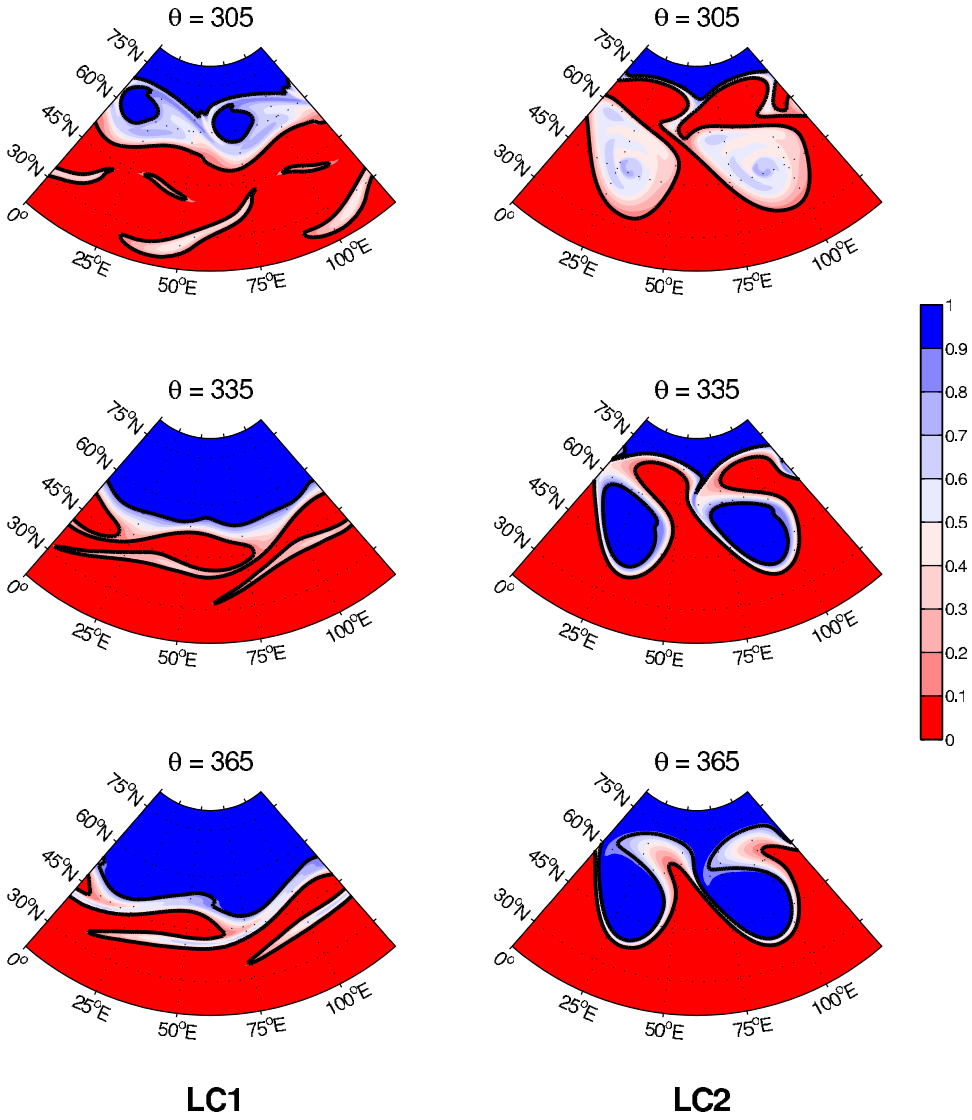

Figure 9. The tracer S_i (i = 1, 2, 3) at day 9, on the isentropic surfaces θ = 305, 335, and 365 K, respectively, from the T170L120 solutions. Left column for the LC1 life cycle, right column for LC2. Black lines indicate the mixing region, as in Figure 7. Projection as in Figure 4.

troposphere, by comparing the relative contribution of each layer ($S_i \rightarrow \mathcal{T}$). Conversely $T_i \rightarrow \mathcal{S}$ can be used to assess the tropospheric origin of air entering the stratosphere.

[47] As can be seen in Figure 8, $S \rightarrow \mathcal{T}$ comes mostly from the 290–320 K isentropic layer (i.e., from $S_1 \rightarrow \mathcal{T}$) for both life cycles. By contrast, $T \rightarrow \mathcal{S}$ is more complicated: for LC1 most transport into the stratosphere occurs in the lower isentropic layer, while for LC2 $T \rightarrow \mathcal{S}$ is relatively independent of height, at least by the end of the life cycle. However, for LC2 a noticeable peak, particularly for $T_1 \rightarrow \mathcal{S}$, appears between 7 and 9 days.

[48] In order to understand these features, one needs to examine the details of the tracer evolution at different heights in the middleworld. This is done in Figure 9, the tracers S_i (i = 1, 2, 3) in the middle of their respective layers, i.e., on θ = 305, 335 and 365 K, are shown at day 9 in the life cycle. Again, blue indicates stratospheric air, red tropospheric air, and white mixed air. The black lines demarcate the mixing region, as in Figure 7.

[49] For the LC1 life cycle (left column in Figure 9), the tracers exhibit substantial vertical structure, as already noted. First, the anticyclonic filaments of stratospheric air are seen to be quite deep, and extend all the way up into the 350–380 K layer. Second, on the 305 K surface very prominent *cyclonic* circulations are apparent, located at high latitudes, and resulting in the development of cutoff cyclonic vortices, smaller yet very similar to those typically accompanying life cycles of type LC2. These high latitude cyclones in LC1, which are also visible in the PV plot in top left panel of Figure 4, are responsible for the relatively large value of $T_1 \rightarrow \mathcal{S}$ compared to the other layers (cf. Figure 8b). Note that, although these cyclones are shallow and confined below 320 K, the air in the mixing region surrounding them is predominantly blue (top left panel of Figure 9), indicating that tropospheric air has been mixed into the stratosphere.

[50] For the LC2 life cycle, in contrast, the cyclonic cutoff vortices are very deep and appear to be vertically aligned. The fate of the air in the cutoff vortices differs

greatly depending on its vertical location in the middle-world. In the lowest layer the cutoff stratospheric air is substantially mixed with tropospheric air, and eventually ends up in the troposphere; this explains both the larger values of $S_1 \rightarrow \mathcal{T}$ for LC2 (cf. Figure 8a), and the relative independence of $T_i \rightarrow \mathcal{S}$ among the three layers at late times (cf. Figure 8b, red curves). Finally, the peak in $T_1 \rightarrow \mathcal{S}$ in Figure 8b around day can be understood as follows: the mixed air within the cutoff vortices in the 290–320 K layer is initially classified as being in the stratosphere (because $S > 0.5$), but is subsequently reclassified as tropospheric as the vortices are further diluted (once $S < 0.5$). This is why the peak around day 8 is followed by lower values at later times.

5. Transport of Boundary Layer Air Into the Free Troposphere and the Stratosphere

[51] The second main issue that we wish to carefully examine in the context of idealized baroclinic life cycles is the lifting of boundary layer air into the free troposphere and the stratosphere. The rate at which boundary layer air is uplifted is an important quantity, as it controls the impact of short-lived anthropogenic and other near-surface emissions on the chemistry of the free troposphere. Some boundary layer air is also known to reach the stratosphere: the amount, the pathways, and the relevant timescales of this transport are all of much interest, because many short-lived species with a potentially significant impact on stratospheric ozone chemistry are emitted in the boundary layer (e.g., "very short-lived halogenated species", *Law et al.* [2007]). Again, we seek to describe and quantify the differences in such transport between the two canonical life cycle types.

[52] We start by defining the free troposphere, denoted by $\mathcal{F}$, as the region where the geopotential height is greater than 2.5 km (To be absolutely precise, the region $\mathcal{F}$ thus defined should be referred to as "the free atmosphere", since it extends to the model top. However, the fraction reaching the stratosphere is minute, as will be shown below. Hence there is no need to burden the definition of $\mathcal{F}$ by specifying a complicated upper boundary.). The transport from the boundary layer into $\mathcal{F}$ is then computed via the quantities

$$B_x \rightarrow \mathcal{F} = \int_{\mathcal{F}} B_x \, \rho dV \tag{18}$$

for each life cycle, where B_x is one of the three boundary layer tracers B_+, B_0, B_- defined in Table 2 and illustrated in Figure 5. These quantities are normalized by the total mass of each layer, i.e., the initial value of

$$\int_{\mathcal{A}} B_x \, \rho dV \tag{19}$$

where $\mathcal{A}$ is the entire atmosphere (north of 15°N).

[53] In Figure 10a the percentage of the initial mass uplifted into $\mathcal{F}$ during each life cycle is shown as a function of time. The results were found to be largely independent of model resolution; hence only the T170L120 results are shown. The key result is immediately apparent: the percentage of uplifted tracer is roughly the same for LC1 (blue) and

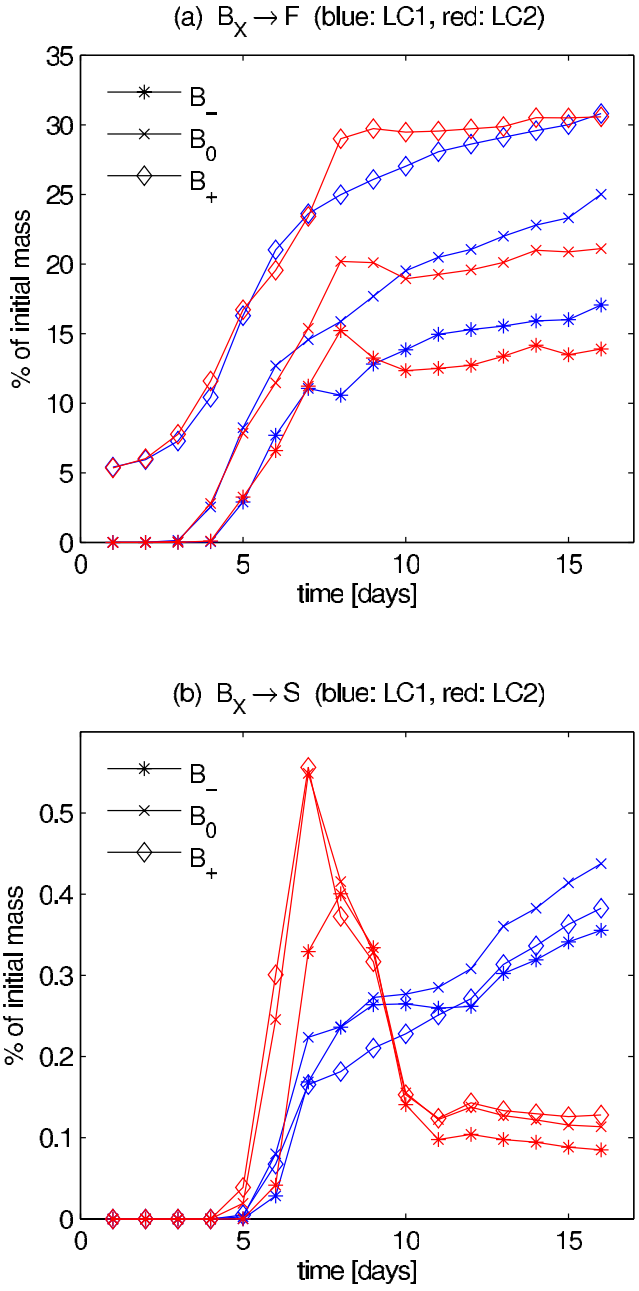

Figure 10. Transport of boundary layer tracer into (a) the free troposphere [$B_x \rightarrow \mathcal{F}$] and (b) the stratosphere [$B_x \rightarrow \mathcal{S}$], as a percentage of the initial mass of tracer in each layer. Blue lines for LC1, red lines for LC2. Different curves indicate different boundary layer tracers, as defined in Table 2, and illustrated in Figure 5.

LC2 (red) life cycles. We submit that transport of boundary layer air into the free troposphere must be largely controlled by the amplitude of the developing baroclinic waves. As can be seen in Figure 10a, the bulk of the transport out of the boundary layer is complete by day 8, and up to that time the EKE is nearly identical for the two life cycles (cf. Figure 3); hence comparable amounts of boundary layer tracer are uplifted into the free troposphere. This also explains the insensitivity to numerical resolution. This behavior should

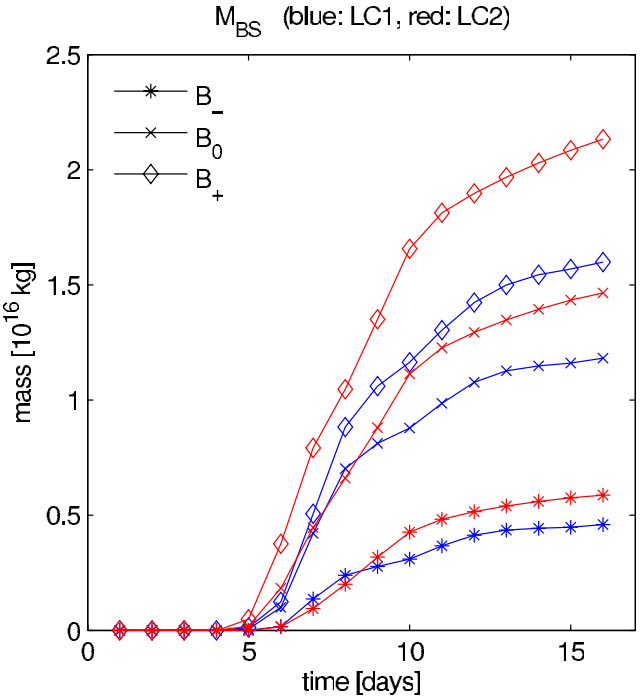

Figure 11. Mixing M_x^{BS} of boundary layer tracers B_x and stratospheric tracer S, as defined in Equation (21). Blue lines for LC1, red lines for LC2. Different curves indicate different boundary layer tracers, as defined in Table 2, and illustrated in Figure 5.

be contrasted the results from stratosphere-troposphere exchange reported above: in that case the transport is controlled by the local kinematics of the flow near the tropopause, yielding very different results between the two life cycles. Finally, we note the unsurprising dependence of $B_x \rightarrow \mathcal{F}$ on the initial distance from the surface, that is to say $(B_+ \rightarrow \mathcal{F}) > (B_- \rightarrow \mathcal{F})$.

[54] We next examine the transport from the boundary layer into the stratosphere by computing the quantity

$$B_x \rightarrow \mathcal{S} = \int_{\mathcal{S}} B_x \ \rho dV \tag{20}$$

which again we normalize by the initial mass of B_x, as defined in Equation (19).

[55] In Figure 10b the quantity $B_x \rightarrow \mathcal{S}$ is plotted for each life cycle. Interestingly, the percentage of boundary layer tracer reaching the stratosphere is largely independent of the precise level of origin within the boundary layer, in contrast to $B_x \rightarrow \mathcal{F}$. Furthermore, there are substantial differences between the two life cycles: approximately four times as much boundary layer tracer reaches the stratosphere for the LC1 life cycle. Note how the curves in Figure 10b, including the peak in transport around day 8 in LC2, follow very similar patterns to those of the quantity $T_1 \rightarrow \mathcal{S}$, shown in Figure 8b. This is not surprising, and simply indicates that the transport into the stratosphere taking place in the 290−320 K layer includes some boundary layer air.

[56] In addition to the relative amount of tracer transported out of the boundary layer, it is worth examining the actual mixing that takes place between boundary layer and stratospheric air. Mixing between near surface pollutants and stratospheric air rich in ozone and NO_y may be responsible for anomalous chemistry and the extent and location of this is therefore of interest. From a chemistry perspective, the natural quantity to compute is the simple product of two species. Hence we quantify the amount mixing between boundary layer and stratospheric air by computing the quantity

$$M_x^{BS} = \int_{\mathcal{A}} SB_x \ \rho dV \tag{21}$$

where, again, B_x stands for any of the three boundary layer tracers B_+, B_0 and B_-. We stress that M_x^{BS} measures the total mixing between boundary layer and stratospheric air as the life cycle develops, whereas the quantity $B_x \rightarrow \mathcal{S}$, is a measure of the injection of boundary layer air into the stratosphere. The former is the relevant quantity if one is interested in quantifying the potential for anomalous chemistry throughout the atmosphere; the latter if one is interested in the impact of transported boundary layer on the composition of the lowermost stratosphere.

[57] As one can seen from Figure 11, irrespective of the initial location of the tracers above the surface, the mixing of boundary layer air with stratospheric air is roughly 20% to 30% greater in the case of LC2 life cycles. This is perhaps surprising, give the fact that the mass of uplifted boundary layer air is roughly identical between the two life cycles. To elucidate this difference, one needs to understand the detailed kinematics of the flow on the relatively low (290−310 K) isentropic levels, which intersect both the boundary layer and the stratosphere (in our initial condition the 320 K surface is above the boundary layer, cf. Figure 5).

[58] In Figure 12 the two tracers B_+ (red) and S_1 (blue) are shown on the 300 K surface, for both life cycles, at selected days. Early in the evolution (days 4), the two tracers are well separated as S is descending while B_+ is being uplifted on the latitudinally sloping isentrope. At this time one can also clearly see the anticyclonic advection of B_+ in LC1, and the cyclonic advection in LC2. By day 6 the mixing begins, as blue and red air masses come together and the gradients steepen. As will be illustrated in the next section, the region of steep gradients along which the two different air masses are coming into contact coincide with the upper level fronts observed within extra-tropical cyclones. Notice how *both* cyclonic and anticyclonic advection is clearly occurring in both life cycles, but LC2 is dominated by cyclonic advection at this level, whereas LC1 exhibits a comparable amount of each.

[59] On day 8, the topology of mixing is becoming clear. To highlight the location where mixing is occurring, we have shaded in grey the regions where the product $S \times B_+ > 0.1$: these are the mixing regions. For LC1, the mixing region is relatively small, and largely confined to the high latitude boundary between the stratospheric and boundary layer air. For LC2, in contrast, the mixing is more vigorous, and occurs because the strong cyclonic circulations wrap the descending stratospheric air and the ascending boundary

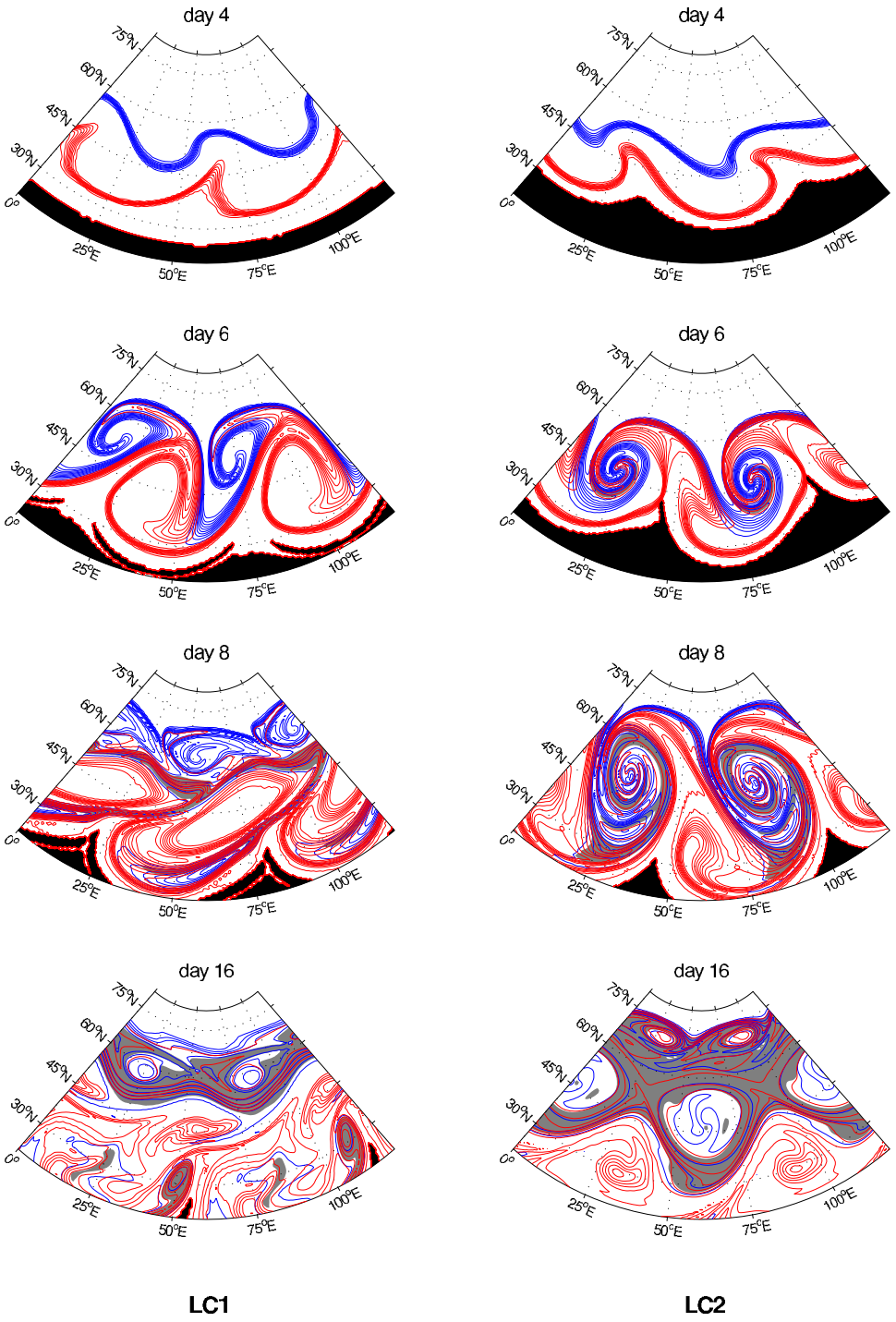

Figure 12. Tracer evolution, at selected days, on $\theta = 300$ K (T170L120 solution); left column for LC1, right column for LC2. Red contours show tracer B_+, blue contours tracer S_1: the contour interval is 0.1 for both. Grey shading: the mixing region (i.e., $(S_1 \times B_+) > 0.1$). Black shading: where the θ surface is below with the ground. Projection as in Figure 4.

layer air into a cyclonic spiral [*Methven and Hoskins*, 1998]. By day 16, the mixing in LC1 is confined to a relatively narrow latitudinal band extending from 55°N to 70°N, which is found to be in the stratosphere: this explains why $B_x \rightarrow \mathcal{S}$ is larger for LC1 than for LC2 (see Figure 10b). For LC2, the much broader mixing region extends from 20°N to 75°N and is located almost entirely in the troposphere, explaining the larger value M_x^{BS} for LC2 (see Figure 11).

6. A 3D View of Air Mass Evolution

[60] Up to this point, tracer evolution has been visualized by two-dimensional snapshots plotted on isentropic surfa-

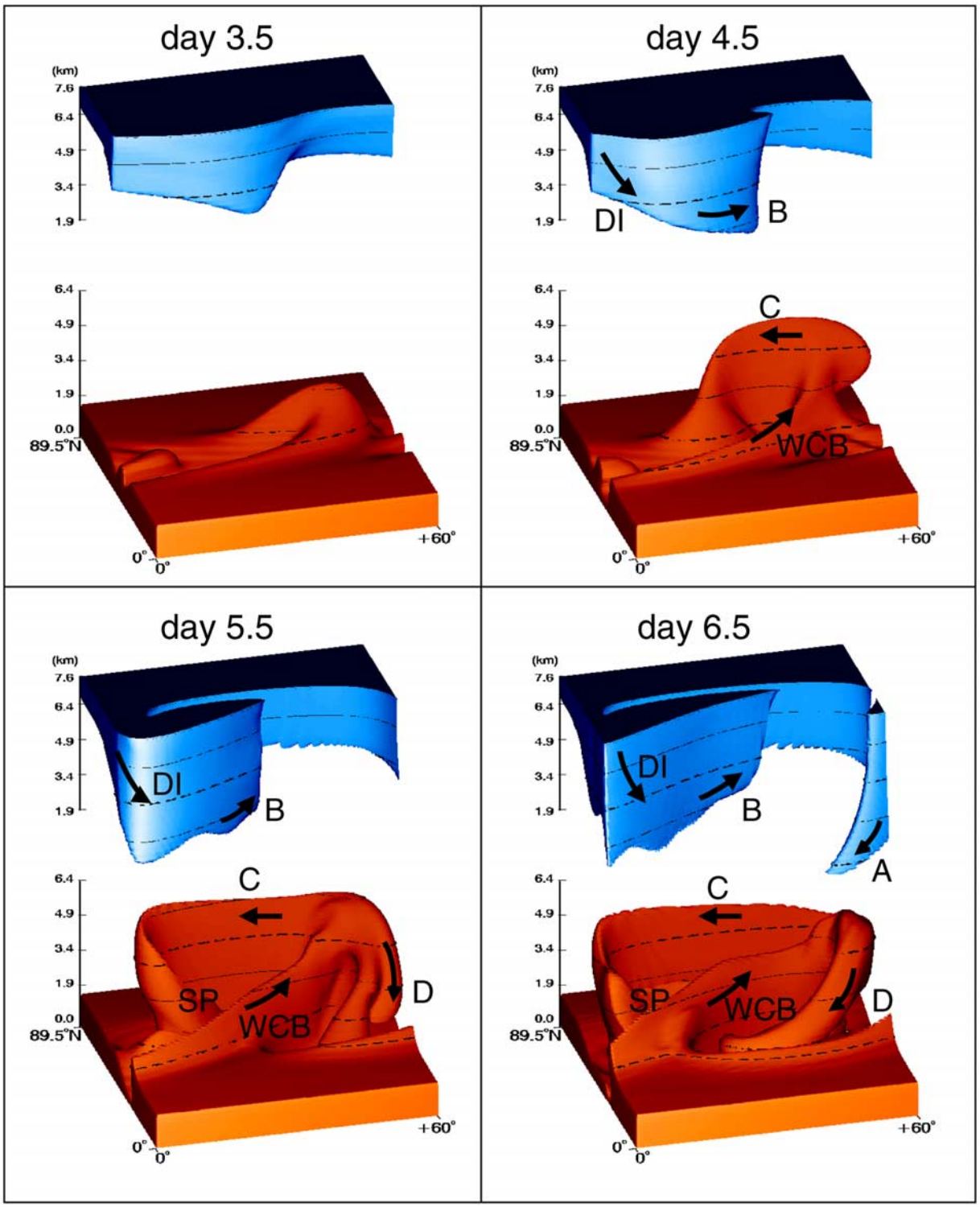

Figure 13. The $B_0 = 0.5$ tracer isosurface (red) and the $S = 0.5$ isosurface (blue) for LC1, between the model surface and 7.6 km (T170L120 solutions). A single period of the developing wave is shown. The red and blue surfaces are here artificially separated by 8 km in z: in fact, the two surfaces are tightly interlocked. Thin black lines: height contours at $z = 1.9$, 3.4, 4.9, and 6.4 km. Labels refer to the different airstreams (see text).

ces: now we turn to three-dimensional pictures. The aim is to present a full 3D view of the air masses and frontal zones, during the life cycles, and capture features that are not immediately apparent in the isentropic plots. In other words, we want to establish what relative air mass flow within a baroclinic wave, sketched by THM in Figure 1, actually looks like by *explicitly computing* it for each life cycle, using the advected tracers. In particular, we wish to deter-

mine the relative positions, orientations and sizes of the airstreams A and B, which develop from the dry intrusion (DI), and C and D, which develop from the warm conveyor belt (WCB).

[61] In Figure 13, isosurfaces of the boundary layer tracer B_0 (in red) and the stratospheric tracer S (in blue) are shown for LC1, at selected days in the life cycle. Several artifices are used to enhance the presentation. First, since the two tracer isosurfaces are deeply interwoven, particularly at later times, an artificial separation of 8 km in the vertical is introduced between them. Second, to aid perspective and indicate the vertical location of the air masses, height contours are plotted on each isosurface (black lines) at 1.9, 3.4, 4.9 and 6.4 km. Third, each panel is shifted in longitude so as to move, approximately, with the phase speed of the baroclinc wave, as it is the relative motion of the airstreams in this frame that is of interest.

[62] All the airstreams illustrated schemetically in Figure 1 can be identified from the tracer isosurfaces shown in Figure 13, and are marked by the corresponding letters. Four key points, which are relatively difficult to deduce from isentropic plots, emerge from this figure:

[63] • Airstream branches appear at different times in the life cycle. The DI and the WCB are clearly apparent by day 4.5, and the uplifted boundary layer air turns cyclonically first, into branch C.

[64] • The DI descending from the stratosphere also turns cyclonically first, clearly forming branch B by day 4.5. The anticyclonic component of the upper level circulation is first evident somewhat later, with branch A only visible after day 6.

[65] • The anticyclonic branch D of boundary layer tracer, also appears later than its cyclonic counterpart C. Its shape is tube-like, qualitatively very different from that of branch C, which appears as a vertically aligned sheet that is progressively strained out.

[66] • The primary location for mixing of boundary layer air and stratospheric air is the spiral denoted SP, in which airstream branches B and C are wound together. This spiral, a cross section of which can be seen more clearly in Figure 12 (day 6, left panel), is actually cyclonic, even though LC1 is characteristically anticyclonic at higher levels.

[67] In Figure 14 the tracer isosurfaces for LC2 are shown. The key differences from LC1 are as follows:

[68] • The WCB is less clearly distinguishable, and is much shorter, at all times in the life cycle.

[69] • The cyclonic air mass branch B emerging from the DI evolves into a deep, vertically aligned, coherent structure. At upper levels it contains purely stratospheric air but, from Figure 12 (day 6 and 8, right panels), we know that its base is a spiral (SP). This spiral has been discussed by *Methven and Hoskins* [1998], and is evident in the PV field (see Figure 4, upper right panel).

[70] • The spiral SP is also evident in the boundary layer isosurface from day 5.5 onwards. It is much larger and deeper than the equivalent structure for LC1 and, again, is the locus where boundary layer and stratospheric air interweave and mix.

[71] • Airstream D appears later than for LC1, at day 6.5, and is oriented NW-SE instead of NE-SW, although it still has a tube-like structure.

[72] • The upper level anticyclonic airstream A never appears. Hence the upper level warm front is between air mass D and the DI in LC2, instead of between air masses D and A in LC1.

7. Summary and Discussion

[73] The results detailed above allow us to answer the specific questions posed in the introduction. We briefly summarize, in turn, what we have learned about stratosphere-troposphere exchange, the fate of boundary layer air, and the three dimensional evolution of the distinct air masses during canonical baroclinic life cycles, and then offer some possible consequences of our findings as they relate to future climate changes.

[74] Stratosphere-troposphere exchange differs in a number of ways between the two life cycles. First the amount of stratosphere to troposphere ($S \rightarrow \mathcal{T}$) transport is found to be around 50% greater in LC2 compared with LC1, whereas total troposphere to stratosphere ($T \rightarrow \mathcal{S}$) transport is roughly comparable between the life cycles. Second the qualitative nature and hence the vertical structure of the transport differs markedly between the two life cycles. In LC2 large, deep cyclonic vortices stir up a broad surf zone where stratospheric and tropospheric mix; at upper levels (335 K–365 K) this surf zone mixing contributes to both $S \rightarrow \mathcal{T}$ and $T \rightarrow \mathcal{S}$, whereas at low levels (305 K) the vortices are eventually entirely mixed into the tropospheric background, thereby yielding larger overall $S \rightarrow \mathcal{T}$ for LC2. In LC1, by contrast, less net $S \rightarrow \mathcal{T}$ transport occurs at upper levels, with only thin anticyclonic filaments of stratospheric air diluted into the troposphere; at lower levels stratospheric filaments are still present, but smaller, shallower cyclonic vortices also form, and they substantially contribute to both $S \rightarrow \mathcal{T}$ and $T \rightarrow \mathcal{S}$. The two-way exchange by these vortices explains why LC1 is found to have a higher ratio of $(T \rightarrow \mathcal{S})/(S \rightarrow \mathcal{T})$ than LC2 (0.40 versus 0.27). The deeper structure of $(T \rightarrow \mathcal{S})$ in LC2 compared to LC1 (cf. Figure 9b) has implications for determining the depth of the 'extratropical tropopause layer' observable in chemical measurements [*Fischer*, 2000; *Hoor et al.*, 2002; *Pan et al.*, 2004]: a deeper extratropical tropopause layer might result if a future climate favored LC2 over LC1.

[75] The net uplift of boundary layer air into the free troposphere ($B_x \rightarrow \mathcal{F}$) is found to be closely comparable between the two life cycles. Linear theory suggests a simple explanation: vertical velocities in the developing life cycles are proportional to wave amplitude, and wave amplitudes are similar for the two life cycles (cf. the comparison of EKE in Figure 3). In contrast, much more boundary layer air is injected directly into the lowermost stratosphere ($B_x \rightarrow \mathcal{S}$) during LC1 than during LC2 (approximately four times more). Extratropical cyclones closely resembling the canonical LC1 type may therefore inject boundary layer chemicals directly into the extratropical tropopause layer, with strong implications for its chemical constitution. However, the total mixing between boundary layer and stratospheric air was found to be approximately 30% higher (as measured by M_0^{BS}) during LC2 than during LC1. For LC2, nearly all of the mixed air ends up in the troposphere, and most of the mixing occurs within the large spiral structure located at the

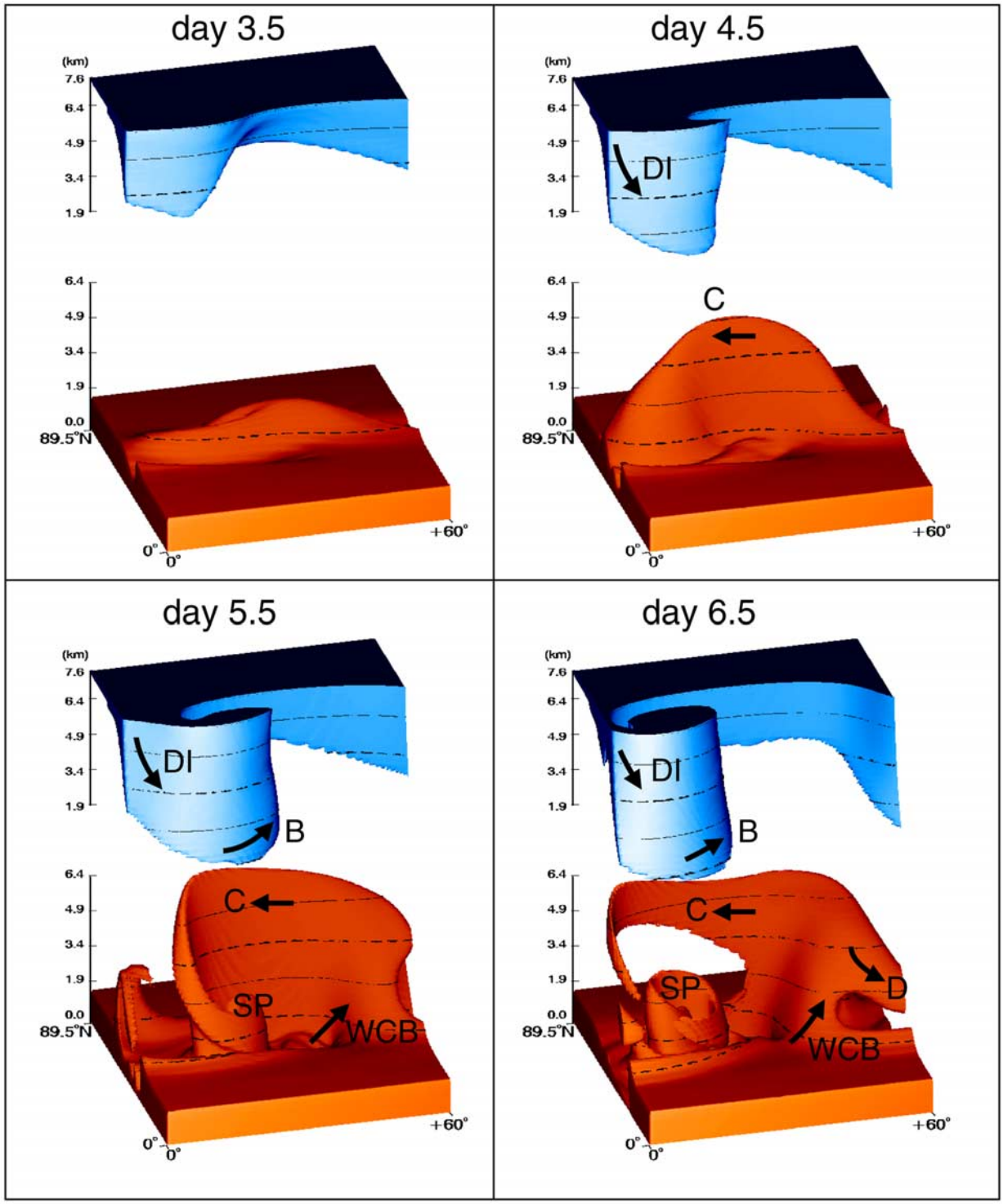

Figure 14. As in Figure 13, but for LC2.

base of the cut-off vortex (feature SP in Figure 14). Such mixing may result in anomalous chemistry as dry, ozone and NO_y-rich stratospheric air encounters moist boundary layer air that could contain recent surface emissions.

[76] Finally, we have used the calculated tracer fields to *compute* three-dimensional pictures (Figures 13 and 14) of relative flow within the baroclinic waves, to compare with the THM schematic (Figure 1), and illustrate the 3D geometries of the different airstream. All of the THM airstream branches are clearly identifiable from the tracer isosurfaces in LC1, whereas in LC2 airstream A is absent, airstream D is weaker and oriented differently, and airstreams B and C are stronger. In both types of life cycle, much of the mixing between boundary layer and stratospheric air takes place in cyclonic spirals, where airstreams B and C are stirred together and mix, with the spiral much deeper and broader in LC2. These spirals, which correspond in observations to the 'comma head' of the comma cloud

pattern [*Carlson*, 1980], should therefore be of particular interest for targeted observation campaigns aimed at understanding mixing and its wider implications.

[77] Having summarized the key results of our idealized study, we now mention its limitations. Clearly, its main weakness is that the mixing of air masses in our model only occurs through the numerical dissipation of the advection scheme. We have checked that our results are insensitive to the specifics of the scheme, by repeating some of the calculations with a piecewise parabolic scheme (instead of the Van Leer scheme). However, in the atmosphere, actual physical processes are believed to be responsible for the mixing of distinct air masses, e.g., moist convection or breaking gravity waves. Because of this, actual mixing rates in the atmosphere might be quite different from the ones in our model, and also spatially inhomogeneous. For instance, convection is likely to occur within the warm conveyor belt, greatly enhancing vertical mixing there. However, we believe that the present study has considerable value, in that it establishes what one might think of as the large scale, dry, adiabatic limit. We submit that this needs to be understood first, if one wishes to evaluate the individual contributions of more complex, smaller scale, less well understood, and often poorly parameterized physical processes.

[78] Aware of the limitations of our study, we conclude by mentioning how the key results of our work might be relevant to future climates. More specifically, we argue that our results are directly relevant to some recent studies, where the possibility of future changes in the relative frequency of LC1 versus LC2 type extratropical cyclones has been raised.

[79] Notably, *Shapiro et al.* [2001] have shown that the relative frequency of LC1 to LC2 in the central and eastern North Pacific storm track is significantly modulated by El Niño and the Southern Oscillation. Specifically, an increased occurrence of LC2 life cycles was observed during the 1997–1998 El-Niño, and of LC1 life cycles during the 1999 La Niña. These observations were found to be accompanied by changes to the mean position of the tropospheric jet in the North Pacific over those periods (see also *Martius et al.* [2007]), suggesting that any climatic change to the jet location may be associated with a change in the preferred type of life cycle. Our findings suggest that one might expect accompanying changes in stratosphere-troposphere exchange, as LC2 life cycles entail a substantial increase in stratosphere to troposphere transport. In fact, evidence for such changes in transport across the tropopause are already appearing. *Zeng and Pyle* [2005] recently demonstrated, using a chemistry-climate model, that a significant increase in transport of stratospheric ozone into the troposphere occurred during the 1997–1998 El Niño. Our results provide an explanation: El Niño is associated with more LC2 life cycles, each of which contributes to increased $S \rightarrow \mathcal{T}$, resulting in larger transport of stratospheric ozone into the troposphere.

[80] Nor is the association between jet position and cyclone life cycle behavior confined to the Pacific. The positive phase of the North Atlantic Oscillation (NAO) has been correlated with anticyclonic wave breaking at the tropopause (i.e., LC1), and the negative phase with cyclonic breaking (LC2) [*Benedict et al.*, 2004; *Franzke et al.*, 2004; *Martius et al.*, 2007]. This is particularly significant as a positive climate-change related trend in the NAO index has been reported [*Thompson et al.*, 2000]. Our results suggest that an increased occurrence of LC1 life cycles, associated with the positive NAO, might result in a decreased stratosphere to troposphere transport and an increase in the direct injection of boundary layer air into the lowermost stratosphere.

Appendix A: Balanced Initialization

[81] We are aware of one procedure for constructing balanced initial conditions, to be found in Appendix II of *Hoskins and Simmons* [1975]. That scheme starts from a given temperature field and derives a correspondigly balanced wind field. However, that scheme relies heavily on the vorticity-divergence formulation of a semi-implicitly time stepped spectral model with finite difference discretization in the vertical; as such, it hard see how one might generalize it to other numerical schemes (e.g., those that use a velocity formulation instead of a vorticity-divergence one). Furthermore, that method recessitates the minimization of a numerically generated two-grid wave in the vertical with a smoothing filter, obviously an undesirable feature.

[82] Here, we present a method for computing balanced initial conditions that is completely independent of the spatial or temporal discretization used by the model. Our method is based solely on the equations of motion and, while requiring a nonlinear iterative solver like the method by *Hoskins and Simmons* [1975], is completely general in its formulation.

A1. Temperature

[83] In order to generate the initial balanced fields, it is helpful to proceed from the pressure-coordinate version of the primitive Equations (1). Given the initial winds, the initial balanced temperature T, is computed from the expression

$$\frac{\partial T}{\partial \phi} = -\frac{H}{R}(af + 2u\tan\phi)\frac{\partial u}{\partial z} \tag{A1}$$

obtained by combining the meridional momentum balance

$$(af + u\tan\phi)u = -\frac{\partial \Phi}{\partial \phi} \tag{A2}$$

with the hydrostatic relation

$$\frac{\partial \Phi}{\partial z} = \left(\frac{R}{H}\right)T \tag{A3}$$

to eliminate the geopotential Φ. Note that the latitudinal derivatives in (A1) and (A2) are taken at constant pressure (or, equivalently, log-pressure z, and not at constant σ).

[84] Equation (A1) is easily integrated to yield

$$T(\phi, z) = T_r(z) - \frac{H}{R}\int_0^{\phi}(af + 2u\tan\phi')\frac{\partial u}{\partial z}\, d\phi' \tag{A4}$$

where $T_r(z)$ is a reference profile, which we choose of the form

$$T_r(z) = T_0 + \frac{\Gamma_0}{(z_T^{-\alpha} + z^{-\alpha})^{1/\alpha}} \tag{A5}$$

where the parameters T_0, Γ_0, z_T and α are given in Table 1. Without introducing discontinuities, this expression gives a simple profile which starts with a value T_0 at the surface, linearly decreases with a constant lapse rate Γ_0 up to a height $z = z_T$, and is uniform above z_T. The parameter α controls the sharpness of the transition from a linear to a uniform profile around z_T. We chose $\Gamma_0 = 6.5$ K/km, as in US 1976 Standard Atmospheric Temperature profile, and $T_0 = 300$ K, which is appropriate for the equator.

[85] We note that the integration in (A4) can be performed very accurately (the zonal wind is known analytically, and thus no numerical differentiation is needed to evaluate the integrand). We do this using Gaussian quadratures, and can obtain machine precision accuracy with about 100 Gaussian points.

A2. Surface Pressure

[86] As can be seen from (1), p_s is a prognostic variable and thus needs to be initialized. In the LC1 case, for which the initial zonal winds vanish at the surface, it suffices to set $p_s = p_0 = 1000$ hPa. In the LC2 case, however, the initial winds u_2 are nonzero at the surface: setting $p_s = p_0$ would yield an unbalanced initial condition if $\Phi = 0$ at the surface as well. Hence prior to computing the balanced initial temperature field as described above, the surface pressure $p_s(\phi)$ must be initialized in order to satisfy

$$\Phi(\phi, p_s(\phi)) = 0 \qquad \text{for all } \phi. \tag{A6}$$

For the specified initial wind u_2 given in Equation (8), the geopotential $\Phi = \Phi_r + \Phi_b$. Here $\Phi_r(p)$ is a reference profile in hydrostatic balance (Equation (A3)) with T_r and is computed using Gaussian quadrature from

$$\Phi_r(p) = \int_p^{p_0} \frac{RT_r(p')}{p'}\, dp' \tag{A7}$$

where T_r is the reference profile given in (A5) expressed here as a function of pressure; recall that $z = H \log(p_0/p)$. The other component $\Phi_b(\phi, p)$ is in geostrophic balance with the wind field u_2 and is computed from the integral version of (A2)

$$\Phi_b(\phi, p) = -\int_0^{\phi} (2a\Omega \sin\phi' + u_2 \tan\phi') u_2 \, d\phi' \tag{A8}$$

where $u_2 = u_2(\phi', p)$ is again expressed as a function of p.

[87] Equation (A6) is a implicit nonlinear equation for $p_s(\phi)$, which we solve using the secant method for each grid latitude ϕ independently; convergence is extremely fast (typically, a few iterations). In fact, one could avoid numerical root-finding procedures completely, and solve for $p_s(\phi)$ explicitly using a one-term Taylor expansion of (A6) about $p_s = p_0$; this much simpler method yields surprisingly accurate results.

[88] Once $p_s(\phi)$ has been calculated, the value of pressure p (and thus log-pressure z) is known at each model grid point (ϕ, σ), and the integral in (A4) is then evaluated at that pressure to compute the balanced temperature T.

[89] **Acknowledgments.** LMP is supported, in part, by the US National Science Foundation, and JGE would like to thank the Nuffield Foundation. The authors wish to express their gratitude to Isaac Held and the staff of NOAA's Geophysical Fluid Dynamics Laboratory, where the computations where performed, Joe Tribbia for illuminating insights on balanced initialization, R. Saravanan for helpful discussions on initial tropopause definition, and C. Jablonowski for a careful reading of the Appendix. LMP also wishes to thank the staff of the Morgan Stanley Children's Hospital of the New York-Presbyterian Medical Center, where this paper was written.

References

Benedict, J. J., S. Lee, and S. B. Feldstein (2004), Synoptic view of the North Atlantic Oscillation, *J. Atmos. Sci.*, *61*, 121–144.

Berthet, G., J. G. Esler, and P. H. Haynes (2007), A Lagrangian perspective of the tropopause and the ventilation of the lowermost stratosphere, *J. Geophys. Res.*, *112*, D18102, doi:10.1029/2006JD008295.

Bethan, S., G. Vaughan, C. Gerbig, A. Volz-Thomas, H. Richer, and D. A. Tiddeman (1998), Chemical airmass differences near fronts, *J. Geophys. Res.*, *103*, 13,413–13,438.

Browning, K. E. (1990), Organisation of clouds and precipitation in extratropical cyclones, in *Extratropical cyclones - The Erik Palmén memorial volume*, pp. 129–153, Am. Meteorol. Soc., Boston, Mass.

Carlson, T. N. (1980), Airflow through midlatitude cyclones and the comma cloud pattern, *Mon. Weather Rev.*, *108*, 1498–1509.

Danielsen, E. F. (1980), Stratospheric source for unexpectedly large values of ozone measured over the Pacific Ocean during Gametag, August 1977, *J. Geophys. Res.*, *85*, 401–412.

Durran, D. R. (1999), *Numerical methods for wave equations in geophysical fluid dynamics*, 465 pp., Springer Verlag, New York.

Esler, J. G., P. H. Haynes, K. S. Law, H. Barjat, K. Dewey, J. Kent, S. Schmitgen, and N. Brough (2003), Transport and mixing between airmasses in cold frontal zones during Dynamics and Chemistry of Frontal Zones (DCFZ), *J. Geophys. Res.*, *108*(D4), 4142, doi:10.1029/2001JD001494.

Fischer, H. (2000), Tracer correlations in the northern high latitude lowermost stratosphere: Influence of cross-tropopause mass exchange, *Geophys. Res. Lett.*, *27*, 97–100.

Franzke, C., S. Lee, and S. B. Feldstein (2004), Is the North Atlantic Oscillation a breaking wave?, *J. Atmos. Sci.*, *61*, 145–160.

Galewsky, J., A. H. Sobel, and I. M. Held (2005), Diagnosis of subtropical humidity dynamics using tracers of last saturation, *J. Atmos. Sci.*, *62*, 3353–3367.

Gettelman, A., and A. H. Sobel (2000), Direct diagnoses of stratosphere-troposphere exchange, *J. Atmos. Sci.*, *57*, 3–16.

Hartmann, D. L. (2000), The key role of lower-level meridional shear in baroclinic wave life cycles, *J. Atmos. Sci.*, *57*, 389–401.

Hintsa, E. J., et al. (1998), Troposphere-to-stratosphere transport in the lowermost stratosphere from measurements of H_2O, CO_2, N_2O and O_3, *Geophys. Res. Lett.*, *25*, 2655–2658, doi:10.1029/98GL01797.

Holton, J. R., P. H. Haynes, M. E. McIntyre, A. R. Douglass, R. B. Rood, and L. Pfister (1995), Stratosphere-troposphere exchange, *Rev. Geophys.*, *33*, 403–439.

Hoor, P., H. Fischer, L. Lange, J. Lelieveld, and D. Brunner (2002), Seasonal variations of a mixing layer in the lowermost stratosphere as identified by the CO-O_3 correlation from in situ measurements, *J. Geophys. Res.*, *107*(D5), 4044, doi:10.1029/2000JD000289.

Hoskins, B. J. (1991), Towards a PV-θ view of the general circulation, *Tellus*, *43AB*, 27–35.

Hoskins, B. J., and A. J. Simmons (1975), A multi-layer spectral model and the semi-implicit method, *Q. J. R. Meteorol. Soc.*, *101*, 637–655.

Law, K. S., et al. (2007), Very short-lived halogen and sulfur substances, Chapter 2 in Scientific assessment of ozone depletion: 2006, Global ozone research and monitoring project, Report no. 50, *Tech. Rep.*, World Meteorological Organization, Geneva.

Lindzen, R. S., and M. Fox-Rabinowitz (1989), Consistent vertical and horizontal resolution, *Mon. Weather Rev.*, *117*, 2575–2583.

Mari, C., M. J. Evans, P. I. Palmer, D. J. Jacob, and G. W. Sachse (2004), Export of Asian pollution during two cold front episodes of the TRACE-P experiment, *J. Geophys. Res.*, *109*, D15S17, doi:10.1029/2003JD004307.

Martius, O., C. Schwierz, and H. C. Davies (2007), Breaking waves at the Tropopause in the Wintertime Northern Hemisphere: Climatological Ana-

lyses of the Orientation and the Theoretical LC1/2 Classification, *J. Atmos. Sci.*, *64*, 2576–2592.
McIntyre, M. E., and T. N. Palmer (1984), The 'surf zone' in the stratosphere, *J. Atmos. Sol. Terr. Phys.*, *46*, 825–849.
Methven, J., and B. J. Hoskins (1998), Spirals in potential vorticity. Part I: Measures of structure, *J. Atmos. Sci.*, *55*, 2053–2066.
Pan, L. L., W. J. Randel, B. J. Gary, M. J. Mahoney, and E. J. Hintsa (2004), Definitions and sharpness of the extratropical tropopause: A trace gas perspective, *J. Geophys. Res.*, *109*, D23103, doi:10.1029/2004JD004982.
Polvani, L. M., R. K. Scott, and S. J. Thomas (2004), Numerically converged solutions of the global primitive equations for testing the dynamical core of atmospheric GCMs, *Mon. Weather Rev.*, *132*, 2539–2552.
Ray, E. A., F. L. Moore, J. W. Elkins, G. S. Dutton, D. W. Fahey, H. Vömel, S. J. Oltmans, and K. H. Rosenlof (1999), Transport into the Northern Hemisphere lowermost stratosphere revealed by in-situ tracer measurements, *J. Geophys. Res.*, *104*, 26,565–26,580, doi:10.1029/1999JD900323.
Shapiro, M. A., et al. (1999), A planetary-scale to mesoscale perspective of the lifecycles of extratropical cyclones, in *The life cycles of extratropical cyclones*, edited by M. A. Shapiro and S. Geonas, pp. 1228–1251, Am. Meteorol. Soc.
Shapiro, M. A., H. Wernli, N. A. Bond, and R. Langland (2001), The influence of the 1997–9 El Ninõ Southern Oscillation on extratropical baroclinic lifecycles over the eastern North Pacific, *Q. J. R. Meteorol. Soc.*, *127*, 331–342.
Simmons, A. J., and B. J. Hoskins (1977), Baroclinic instability on the sphere: Solutions with a more realistic tropopause, *J. Atmos. Sci.*, *34*, 581–588.
Snyder, J. P., and P. M. Voxland (1994), *An Album of Map Projections*, *USGS Professional Paper 1453*, 249 pp., United States Government Printing Office, New York.
Stohl, A., et al. (2003a), Stratosphere-troposphere exchange: A review, and what we have learned from STACCATO, *J. Geophys. Res.*, *108*(D12), 8516, doi:10.1029/2002JD002490.
Stohl, A., et al. (2003b), A new perspective of stratosphere-troposphere exchange, *Bull. Am. Meteorol. Soc.*, *84*, 1565–1573.
Stone, E. M., W. J. Randel, and J. L. Stanford (1999), Transport of passive tracers in baroclinic wave life cycles, *J. Atmos. Sci.*, *56*, 1364–1381.
Thompson, D. W., J. M. Wallace, and G. C. Hegerl (2000), Annular modes in the extratropical circulation II: Trends, *J. Climate*, *13*, 1018–1036.
Thorncroft, C. D., B. J. Hoskins, and M. E. McIntyre (1993), Two paradigms of baroclinic wave life-cycle behaviour, *Q. J. R. Meteorol. Soc.*, *119*, 17–55.
Vaughan, G., and C. Timmis (1998), Transport of near tropopause air into the lower midlatitude stratosphere, *Q. J. R. Meteorol. Soc.*, *124*, 1559–1578.
von Hardenberg, J., K. Fraedrich, F. Lunkeit, and A. Provenzale (2000), Transient chaotic mixing during a baroclinic life cycle, *Chaos*, *10*, 122–134.
Wang, K.-Y., and D. E. Shallcross (2000), A Lagrangian study of the three-dimensional transport of boundary-layer tracers in an idealised baroclinic-wave life-cycle, *J. Atmos. Chem.*, *35*, 227–247.
Wei, M. Y. (1997), A new formulation of the exchange of mass and trace constituents between the stratosphere and troposphere, *J. Atmos. Sci.*, *44*, 3079–3086.
Wernli, H., and M. Bourqui (2002), A Lagrangian "1-year climatology" of (deep) cross-tropopause exchange in the extratropical northern hemisphere, *J. Geophys. Res.*, *107*(D2), 4021, doi:10.1029/2001JD000812.
Wirth, V., and J. Egger (1999), Diagnosing extratropical synoptic-scale stratosphere-troposphere exchange: A case study, *Q. J. R. Meteorol. Soc.*, *125*, 635–655.
Zeng, G., and J. A. Pyle (2005), Influence of El Ninõ Southern Oscillation on stratosphere/troposphere exchange and the global tropospheric ozone budget, *Geophys. Res. Lett.*, *32*, L01814, doi:10.1029/2004GL021353.

J. G. Esler, Department of Mathematics, University College London, Gower Street, London, WC1E 6BT, England. (gavin@math.ucl.ac.uk)
L. M. Polvani, Department of Applied Physics and Applied Mathematics and Department of Earth and Environmental Sciences, Columbia University, S.W. Mudd, Room 216, 500 West 120th Street, New York, NY 10027, USA. (polvani@columbia.edu)